CHARACTERIZATION OF AAV2-GCAMP3 FOR FUNCTIONAL IMAGING IN RETINAL GANGLION CELLS

by

Delaney Catherine Marie Henderson

Submitted in partial fulfillment of the requirements for
the degree of Master of Science

at

Dalhousie University
Halifax, Nova Scotia
August 2020

Dedication

This thesis is dedicated to my family for their constant and
unwavering love, support, inspiration and encouragement.
Thank you for pushing me to be the best I can be
and for instilling in me a hard work ethic,
and an inquisitive mind.

Table of Contents

List of Tables

List of Figures

Abstract

The loss of retinal ganglion cells (RGCs) is the hallmark of optic neuropathies, such as glaucoma. Monitoring RGC function and subsequent dysfunction over time is an invaluable tool in experimental optic neuropathies and potentially in clinical disease. This research characterizes a non-invasive technique for delivering a functional fluorescent marker to RGCs to optically record function. We tested the hypothesis that the genetically encoded calcium (Ca^{2+}) indictor, GCaMP, could be exogenously delivered to the retina with intravitreal injection and produce functional GCaMP3 proteins capable of responding to external stimuli. C57Bl/6 mice were injected with an AAV2-CAG-GCaMP3 viral vector and monitored weekly with *in vivo* confocal scanning laser ophthalmoscopy over five weeks to quantify the transduction of the virus into retinal cells. Following five weeks, Ca^{2+} imaging was performed in retinas of a subset of mice injected with AAV2-CAG-GCaMP3 and well as in Thy1-GCaMP3 transgenic mice. Transient increases of intracellular Ca^{2+} evoked by 50 μM kainic acid (KA) treatments were recorded. In another subset of AAV2-GCaMP3 injected mice, retinas were processed for immunohistochemistry with antibodies against RBPMS (a marker for RGCs), ChAT (a marker for cholinergic amacrine cells), and GFP (to enhance the GCaMP signal). In all injected mice, labelled cells were visible with *in vivo* imaging one-week following injection. The density of transduced cells increased significantly over five weeks, and the labelling persisted to six-months post-injection. *Ex vivo* Ca^{2+} imaging demonstrated that the transduced GCaMP3 was functional in response to treatments of 50 μM KA. The transduced GCaMP3 produced similar mean KA-induced-transients when compared to Thy1-GCaMP3 transgenic mice. Immunohistochemical analysis determined that a mean (SD) of 79 (6)% of GFP-positive cells were RBPMS-positive, 9 (4)% were ChAT-positive, and 12 (7)% did not co-localize with either RBPMS or ChAT. This research demonstrates that exogenous functional fluorescent markers such as GCaMP can be delivered to the retina, be visualized with *in vivo* imaging and be used to record functional responses from RGCs. It paves the way for examining single cell functional responses, both *in vivo* and non-invasively, for evaluating experimental optic neuropathies and gauging the effects of potential neuroprotective avenues. Finally, it is proof-of-principle for translation to clinical medicine.

List of Abbreviations Used

$[Ca^{2+}]$	Calcium concentration
$[Ca^{2+}]_i$	Intracellular calcium concentration
2P	2-photon
AAV	Adeno-associated virus
AAV2	Adeno-associated virus serotype 2
AAV9	Adeno-associated virus serotype 9
AMPA	α-amino-3-hydroxy-5-methyl-4-isoxazolepropionic acid
AP	Action potential
Au	Arbitrary unit
Ca^{2+}	Calcium
CAG	Cytomegalovirus early enhancer/chicken β actin promoter
CBA	Chicken β-actin promoter
ChAT	Choline acetyltransferase
CSLO	Confocal scanning laser ophthalmoscopy
EPSPs	Excitatory postsynaptic potentials
ER	Endoplasmic reticulum
ERG	Electroretinogram
F_0	Baseline fluorescence
FRET	Fluorescence (Förster) Resonance Energy Transfer
DCX	Doublecortin
GABA	Gamma-aminobutyric acid
GAD	Glutamic acid decarboxylase
GCL	Ganglion cell layer
GECI	Genetically encoded calcium indicator
GFP	Green fluorescent protein
GLYT	Glycine neurotransmitter transporter
HBSS	Hanks balanced salt solution
IFNγ	Interferon γ
IHC	Immunohistochemistry

ILM	Inner limiting membrane
INL	Inner nuclear layer
IOP	Intraocular pressure
IR	Infrared
K^+	Potassium
KA	Kainic acid
LV	Lentivirus
MCU	Mitochondrial Calcium Uniporter
MICU1	Mitochondrial calcium uptake 1
MICU2	Mitochondrial calcium uptake 2
Na^+	Sodium
NAbs	Neutralizing antibodies
NCX	Na^+/Ca^{2+} Exchanger
NDMA	N-methyl-D-aspartate
NFL	Nerve fiber layer
NHP	Non-human primate
OCT	Optical coherence tomography
OGB	Oregon Green BAPTA
ONH	Optic nerve head
ONL	Outer nuclear layer
ONT	Optic nerve transection
OPL	Outer plexiform layer
PBS	Phosphate buffered saline
PFA	Paraformaldehyde
PMCA	Plasma membrane Ca^{2+} ATPase
PRL	Photoreceptor layer
RBPMS	RNA-binding protein with multiple splicing
RGC	Retinal ganglion cell
RNFL	Retinal Nerve Fiber Layer
RPE	Retinal pigment epithelium
ROI	Region of interest

SERCA	Sarco-/endoplasmic reticulum Ca^{2+} ATPase
TTX	Tetrodotoxin
TH	Tyrosine Hydroxylase
Thy1	Thymocyte differentiation antigen 1
VGCC	Voltage gated calcium channel

Acknowledgements

When I began volunteering in the Retina and Optic Nerve Laboratory during my undergraduate degree, I never thought that I would be in this position, having had the innumerable opportunities I have been so fortunate to have experienced. It has definitely taken a village and without the colleagues, mentors and friends along the way, none of the work leading up to this degree, nor this degree itself would have been possible.

To my supervisor, Dr. Balwantray Chauhan, thank you for your knowledge and expertise over the past few years. Thank you for your encouragement, for pushing me to think critically, but most importantly to always be excited by science; you have made me strive to be a better researcher and I am incredibly grateful. It has been a privilege to learn from you and I look forward to continuing to do so and to begin my PhD under your supervision in September 2020.

Thank you to the members of my supervisory committee, Dr. William Baldridge, and Dr. Frank Smith for your support, knowledge, and feedback over the past two years. Your questions, suggestions and guidance, have helped me become a better researcher and neuroscientist.

To Michele Hooper and Dr. Corey Smith; thank you for your help, patience, listening ears, technical advice and tips along the way, and for taking the time to teach me. You both have my deepest appreciation.

To Dr. Spring Farrell, aka lab mom, aka conference wizard, thank you for everything you have done for me over the past five years. From the tissues, to the pep talks, to the successes, I probably would not have made it this far without your support, knowledge and advice on lab and life skills. In addition, I would like to thank my colleague, close friend and part-time office mate Tareq Yousef. Thank you for your constant support, friendship and feedback on early drafts of this thesis. I am so grateful to be able to share this graduate school experience with you.

Finally, thank you to my other friends and colleagues in both the Retina and Optic Nerve Laboratory and the Department of Medical Neuroscience, I appreciate you all.

CHAPTER 1. Introduction

1.1. The Retina

1.1.1. Anatomy of the Retina

Vision allows us to perceive, interpret, and interact with our environment. The visual pathway begins when light rays enter the eye through the pupil. These light rays are refracted twice; first by the cornea, and then by the crystalline lens before they converge onto the retina (Figure 1.1). The retina is a laminated, multi-layered neural tissue responsible for processing visual signals and transmitting this information to the brain.

The retina is composed of five major types of neurons; rod and cone photoreceptors, horizontal cells, bipolar cells, amacrine cells, and retinal ganglion cells (RGCs). These neurons are organized into five distinct anatomical layers (Figure 1.2); three nuclear layers which contain the somatas of the retinal neurons and two plexuses where the dendritic processes of the retinal neurons synapse with each other. The outer nuclear layer (ONL) is the outermost nuclear layer of the retina and is where the cell bodies of the light sensitive rod and cone photoreceptors reside. Moving towards the inner retina, the next nuclear layer is the inner nuclear layer (INL) containing bipolar and amacrine cells. The ganglion cell layer (GCL) is the innermost nuclear layer where RGCs and displaced amacrine cells are found. Between the ONL and INL is the outer plexiform layer (OPL) where rod and cone photoreceptor terminals synapse with horizontal and bipolar cell processes. The inner plexiform layer (IPL) lies between the INL and the GCL and is where bipolar cells and amacrine cells synapse with RGCs. RGCs are the output neuron of the retina. The information they receive is relayed along their axons that largely

compose the retinal nerve fiber layer (RNFL) and optic nerve. The latter exits the eye at the posterior pole and carries visual signals to higher level visual centres in the brain for further processing.

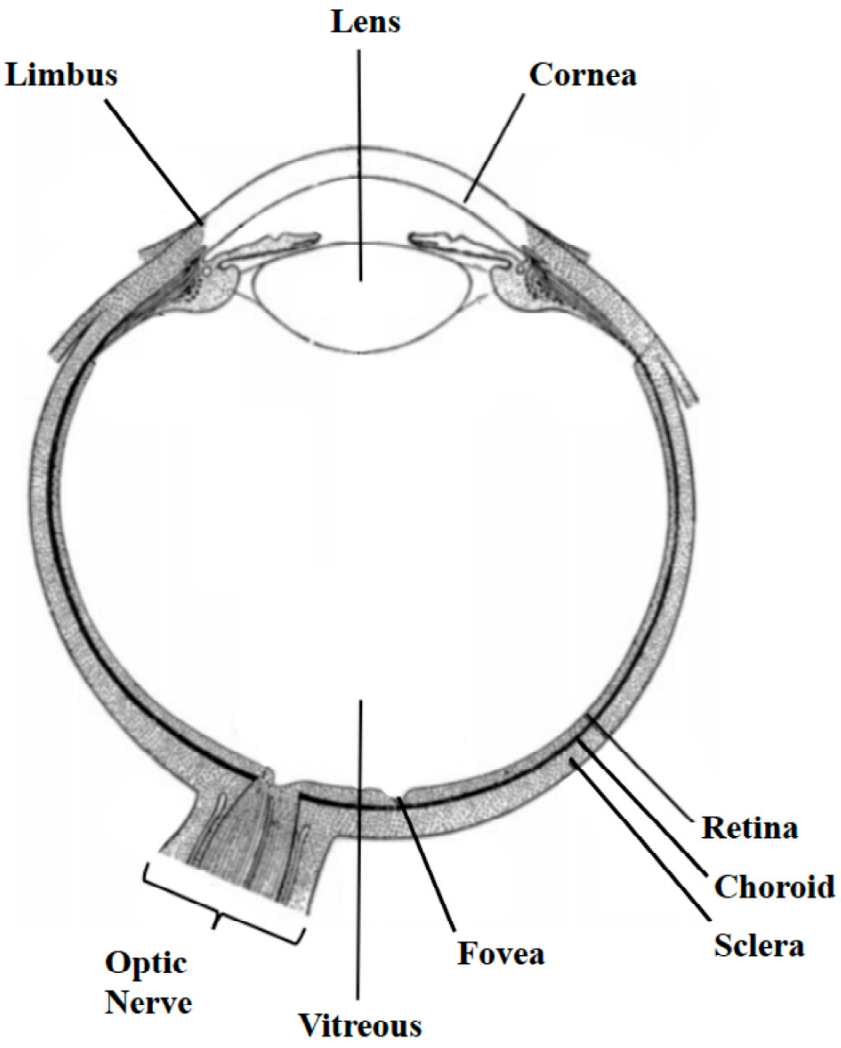

Figure 1.1. Anatomy of the human eye. Figure was adapted from Smerdon, 2011, with permissions.

1.1.2. Signal Propagation through the Retina

Signal propagation through the retina begins when the light rays that enter the eye pass through the retinal layers until they reach the photoreceptor layer (PRL) that is adjacent to the retinal pigment epithelium (RPE). The RPE is a pigmented monolayer that lies between the light sensitive outer segments of rod and cone photoreceptors and the choroid that supplies blood to the outer retina. The RPE acts to supply nutrients to the photoreceptors and plays a critical role in phagocytosing the constantly regenerating rod and cone outer segments as they degenerate due to photo-oxidative damage (Boulton and Dayhaw-Barker, 2001).

Once light excites the photoreceptors, a cascade of reactions through the retina begins. Photons of light cause photoisomerization of rhodopsin and cone opsins, in rods and cones respectively, resulting in the conversion of light into electrical and chemical signals that travel through the retinal layers until they reach the RGCs (Sanes and Zipursky, 2010). Rod and cone outer segments contain photopigments, allowing them to respond to certain wavelengths of light. A photopigment is a molecule which undergoes a chemical reaction in response to certain wavelengths of light. Rod photoreceptors are primarily active in dim light conditions and cone photoreceptors are active in bright light conditions and are also responsible for colour perception. Photoreceptors exist in a constant state of depolarization in the absence of light; therefore, there is a sustained release of glutamate, one of the primary excitatory neurotransmitters in the CNS, onto bipolar cell processes. Upon the detection of photons by their outer segments, the photoreceptors become hyperpolarized. The photon causes the catalysis of 11-cis-retinal into all-trans-retinal which drives downstream reactions leading to a decrease in the

amount of glutamate released by photoreceptors, onto bipolar cell processes in the OPL (Bloomfield and Dowling, 1985).

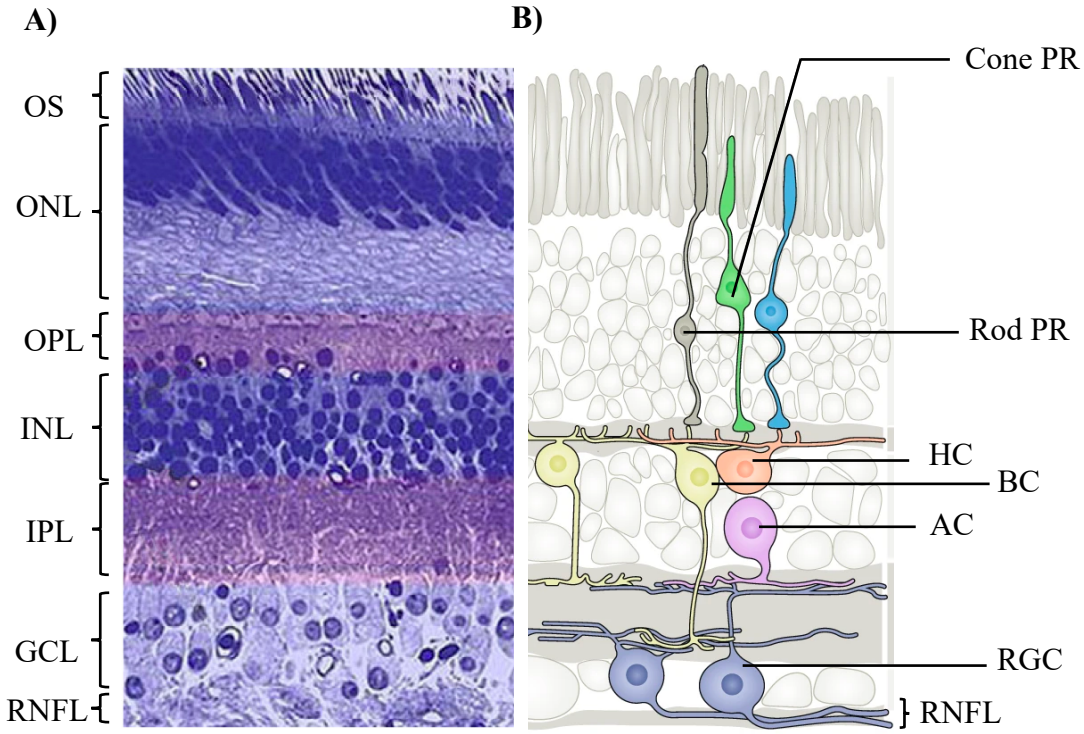

Figure. 1.2. Anatomy of the mammalian retina. A) Nissl stained retinal cross section depicting the three major neuronal layers and two major plexiform layers. The photoreceptor outer segments (OS), the outer nuclear layer (ONL), the outer plexiform layer (OPL), inner nuclear layer (INL), inner plexiform layer (IPL) and ganglion cell layer (GCL). Figure was adapted from Helga Kolb, Webvison the Organization of the Retina and Visual System. 2011. B) Schematic of the five major neurons and their connectivity in the retina. The signal from rod and cone photoreceptors (PRs) is modified by horizontal cells (HCs) and synapse onto bipolar cells (BCs). The signal is further modified by amacrine cells (ACs) before synapsing with retinal ganglion cells (RGCs). Adapted from Baden et al., 2019, with permission.

The main role of bipolar cells is transmitting signals from the photoreceptors to RGCs in a vertical path; all three of which are glutaminergic in vertebrate retinas (Ehinger et al., 1988; Marc et al., 1990). Bipolar cells and their subsequent signalling pathways to RGCs can be classified into two major groups: ON bipolar and OFF bipolar cell pathways (Werblin and Dowling., 1969). In addition to their function in response to light, ON and OFF bipolar cells can also be differentiated by the laminae in which they stratify in the IPL where they synapse onto RGCs (Kolb et al., 2001). In response to light, ON bipolar cells become depolarized, while OFF bipolar cells become hyperpolarized. ON bipolar cells, express a metabotropic glutamate receptor (mGluR6) that is coupled to an inhibitory G protein (Slaughter and Miller, 1983). When glutamate binds, an intracellular cascade occurs, resulting in the closure of voltage-gated ion channels, hyperpolarizing the bipolar cell and reducing the amount of glutamate that is released onto RGCs. OFF bipolar cells, express ionotropic glutamate receptors (AMPA and kainate) that in response to glutamate binding, open non-selective cation channels permeable to potassium (K^+), sodium (Na^+) and calcium (Ca^{2+}; Slaughter and Miller, 1983). Upon glutamate binding, cations can flow into the bipolar cell from the extracellular environment, causing depolarization and subsequent release of glutamate that binds to ligand gated receptors on RGC processes in the IPL.

ON and OFF bipolar cells relay their information onto ON and OFF RGCs that also have morphological and physiological differences. OFF RGCs have processes that stratify into sublamina a of the IPL (more posterior; closer to the bipolar and amacrine cell bodies) where they synapse with OFF bipolar cells (Kolb et al., 2001). In contrast, the ON type RGCs stratify into sublamina b of the IPL (more anterior; closer to the RGC cell bodies) where they synapse with ON bipolar cells. There are also ON-OFF RGCs that are

activated with both the onset and offset of light and have processes that stratify into both sublamina a and b in the IPL (Amthor et al., 1984; Kolb et al., 2001). The electrical signals are propagated along the RGC axon to synapse in the brain; primarily the superior colliculus (SC) in the midbrain of rodents and the lateral geniculate nucleus of the thalamus in primates (Sanes and Zipursky, 2010) where the signals are further processed.

There are two other neurons, classified as interneurons, that are crucial in the modulation of signals that propagate throughout the retina; horizontal and amacrine cells. Horizontal cells interact with photoreceptors, modulating their outputs and are thought to play a role in early visual processing as it pertains to contrast enhancement and opposing colours (Chapot et al., 2017). Horizontal cells also mediate lateral inhibition as they synthesize and release γ-aminobutyric acid (GABA), an inhibitory neurotransmitter, onto photoreceptors (Wässle, 2004) and can act in feedback and feedforward mechanisms (Kolb et al., 2001). Amacrine cells act to modify and integrate the signal between bipolar cells and RGCs, and similar to horizontal cells, are inhibitory in nature, sending inhibitory neurotransmitters, glycine and GABA, onto RGC processes. Although amacrine cells reside primarily in the INL, they can be displaced in the GCL and can make up to 50% of the total neurons residing in the GCL of the mouse retina (Jeon et al., 1998). The number of displaced amacrine cells varies by species and proximity to the optic nerve head (Curcio and Allen, 1990; Jeon, Strettoi and Masland, 1998; Chen and Naito, 1999)

1.2. Calcium

1.2.1. The Role of Calcium in Neurons

Calcium (Ca^{2+}) is a second messenger that is critical for the normal functioning of neurons and is involved in a variety of cellular functions, among which are membrane

excitability, metabolism, vesicle trafficking and gene transcription (Berridge, Lipp and Bootman, 2000). Fundamentally, Ca^{2+} is involved in the transmission of signals via action potentials (APs) within and between neurons. When neurons fire APs, the depolarization causes the opening of voltage gated Ca^{2+} channels (VGCC), allowing Ca^{2+} to flow into the neuron where it is involved in the release of neurotransmitters from synaptic vesicles (Katz and Miledi, 1967; Augustine et al., 1985; Sabatini and Regehr, 1996; Meinrenken et al., 2003). Ca^{2+} aids with the fusion of synaptic neurotransmitter (NT) filled vesicles with the presynaptic membrane through recruiting SNARE proteins that are important for the docking and fusing steps of this release process (Neher and Sakaba, 2008). The vesicle contents are then released into the synaptic cleft where the NTs can bind to other neurons (for review see Südhoft, 2012).

Following neuronal depolarization, Ca^{2+}-activated K^{+} channels act to induce hyperpolarization of the neuron to control neuronal excitability and return it to its resting membrane potential. Ca^{2+} plays an intimate role in shaping APs, and it can contribute to long-term potentiation and long-term depression in neurons; the strengthening of synaptic connections over time from frequent stimulation or the weakening of synaptic strength over time, respectively (Dingeldine et al., 1999; Zucker, 1999; Lüscher and Malenka, 2012). Ca^{2+} is also a key player in gene transcription which occurs primarily through ionotropic and metabotropic glutamate receptor induced Ca^{2+} activity (for extensive review see Lyons and West, 2011). Ca^{2+} has autoregulative properties in that the genes for some of the proteins that control Ca^{2+} within the neuron are controlled by Ca^{2+} itself (Brini and Carafoli, 2009). Therefore, for these critical cellular processes to occur, Ca^{2+} flux must be tightly regulated.

1.2.2. The Regulation of Calcium in Neurons

Under resting conditions, there is a large concentration gradient across the membrane with the intracellular or cytosolic calcium concentration ($[Ca^{2+}]_i$), at approximately 100 nM and the extracellular Ca^{2+} concentration at approximately 2 mM. To ensure this gradient is maintained, Ca^{2+} is tightly regulated through a number of pumps, channels and ATPases both within the neuron, on organelle membranes, and on the plasma membrane (Figure 1.3). Within the neuron, Ca^{2+} is sequestered in the endoplasmic reticulum (ER) and mitochondria. The movement of ions across the membranes of these organelles is regulated through a number of different channels and pumps. The ER contains two types of receptors that, when activated, are responsible for Ca^{2+} release from the ER into the cytosol: ryanodine receptors (RyRs) and inositol-1,4,5-tris-phosphate receptors (IP_3Rs; Henzi and MacDermott, 1992; Kostyuk and Verkhratsky, 1994; Simpson et al., 1995). Sarco-/endoplasmic reticulum Ca^{2+} ATPases (SERCA) permit Ca^{2+} ions to flow into the ER from the cytosol.

RyRs and IP_3Rs both sample information from the ER lumen and the cytosol and are extremely sensitive to fluctuations in $[Ca^{2+}]_i$ as they are both activated by small increases in $[Ca^{2+}]_i$ and are inactivated at high $[Ca^{2+}]_i$ (Meissner, 1986; Bezprozvanny, Watras and Ehrlich, 1991). These receptors can also be activated by Ca^{2+}-induced-Ca^{2+}-release (CICR). CICR is a process in which Ca^{2+} being released from the ER causes local

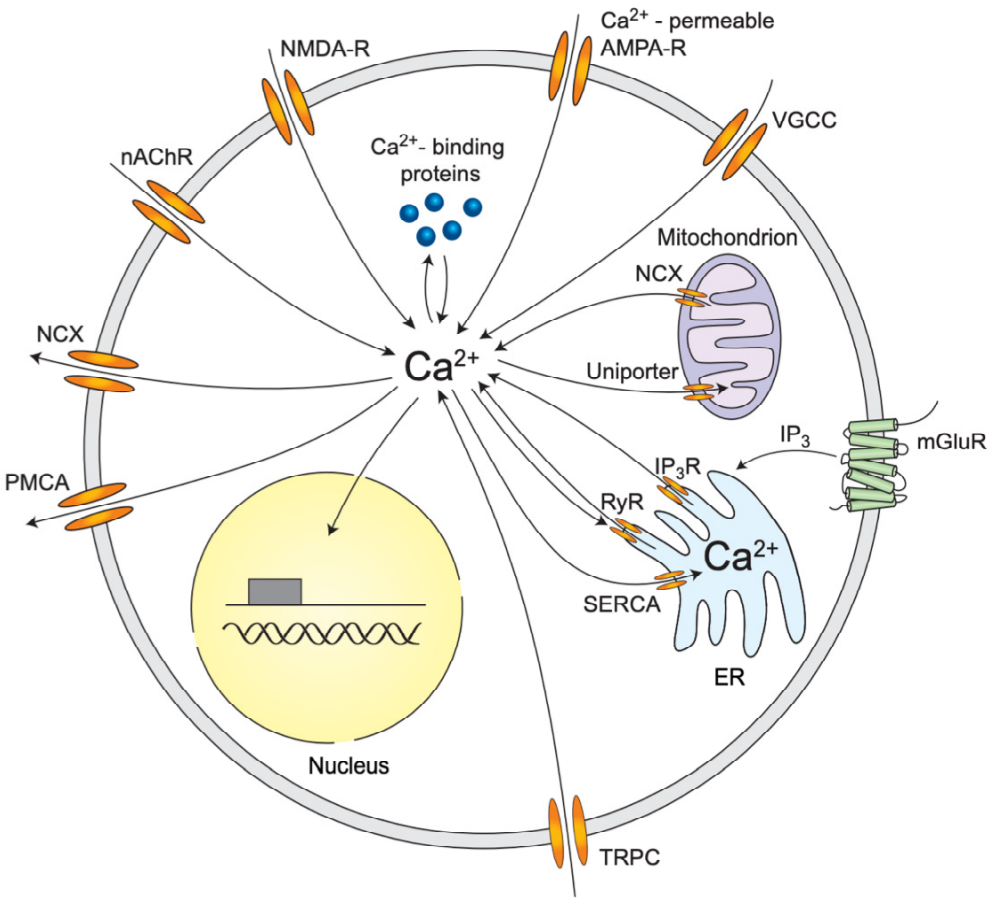

Figure 1.3. Calcium signaling in neurons. Schematic showing the major channels, pumps and ATPases involved in Ca^{2+} dynamics on the plasma membrane of neurons and on organelle membranes. From Grienberger and Konnerth, 2012, with permission.

elevations in [Ca^{2+}] that promotes more Ca^{2+} to be released (Roderick, Berridge and Bootman, 2003). The release of Ca^{2+} by IP_3Rs occurs when phosphatidylinositol 4,5-bisphosphate ($PI[4,5]P_2$) is hydrolyzed into two second messengers: inositol triphosphate (IP_3) and diacylglycerol (DAG), and IP_3 binds to IP_3R and promotes the release of Ca^{2+} into the cytoplasm. Cytosolic Ca^{2+} also activates the channel but when acting together with IP_3, can cause an increase in the activity of the IP_3R receptor (Berridge, 1998). In contrast, the SERCA acts to remove Ca^{2+} from the cytosol, transporting two Ca^{2+} ions into the ER lumen in exchange for three H^+ ions for each ATP hydrolyzed (Brini and Carafoli, 2009).

The mitochondria is another organelle involved in regulating $[Ca^{2+}]_i$. They contain two main mechanisms for Ca^{2+} influx and efflux; the mitochondrial Ca^{2+} uniporter (MCU) and the Na^+/Ca^{2+} exchanger (NCX), respectively. The MCU is involved in the unidirectional entry of Ca^{2+} ions from the cytoplasm into the mitochondria which occurs due to the mitochondrial membrane potential. The electron transport chain exists on the inner membrane of mitochondria and pumps protons from the matrix into the intermembrane space, causing the matrix to adopt an electrochemical gradient of -180 mV (Marchi and Pinton, 2014). Under physiological conditions, the MCU has a low affinity for Ca^{2+}, and can associate with two accessory proteins; mitochondrial calcium uptake 1 (MICU1) and MICU2 which regulate MCUs function via their EF-hand domains that detect Ca^{2+}. At resting state conditions, MICU1 impairs Ca^{2+} flux through MCU into the matrix, however, when there is an increase in cytosolic Ca^{2+}, Ca^{2+} binds to the EF-hand domains and allows for MCU to adopt an open confirmation and Ca^{2+} can flow quickly down its electrochemical gradient into the matrix (Brini et al., 2014). The NCX is also located on the inner mitochondrial membrane and it acts to pump Ca^{2+} out of the

matrix of the mitochondria to the cytosol. It uses secondary active transport, pumping three Na^+ ions into the matrix and one Ca^{2+} ion out, allowing for the maintenance of the mitochondrial electrochemical gradient (Palty et al., 2010; Brini et al., 2014).

There are a number of proteins and channels on the plasma membrane that act to regulate Ca^{2+} efflux and influx between the cytosol and the extracellular environment. The two responsible for the majority of Ca^{2+} efflux are the Ca^{2+} ATPases (PMCA) and the NCXs that remove Ca^{2+} from the cytosol and restore basal Ca^{2+} levels (Berridge et al., 2003). The PMCAs are considered to play a large housekeeping role as they have a high affinity for Ca^{2+} (Brini et al., 2014). They act by way of primary active transport, using the hydrolysis of ATP to allow conformational changes to occur in the protein and the subsequent extrusion of Ca^{2+}. The NCX is known to have a low affinity for Ca^{2+} but a high capacity for Ca^{2+} transport.

There are voltage gated Ca^{2+} channels (VGCCs) and ligand gated plasma membrane channels, which upon activation cause influx of Ca^{2+} into the cell. VGCCs are activated when there are membrane depolarizations, for example in the case of action potentials (AP), allowing Ca^{2+} to flow into the cell and act as a second messenger to propagate and initiate signals within the neuron; turning electrical signals received by the cell into Ca^{2+} transients (Catterall, 2011).

Ligand gated Ca^{2+} channels are activated upon the binding of external molecules from the extracellular space such as glutamate. Glutamate is the primary excitatory neurotransmitter in the CNS and when bound can activate two classes of receptors; the ionotropic receptors and the metabotropic receptors (Brini et al., 2014). The ionotropic receptor family is composed of α-amino-3-hydroxy-5-methyl-4-isoxazolepropionic acid (AMPA), N-methyl-D-aspartate (NMDA), and kainate receptors, named for the

compounds that can activate them. They are typically expressed on neuronal membranes and at glutaminergic synapses and act to produce excitatory postsynaptic potentials (EPSPs) in the postsynaptic neuron (Purves, Augustine, Fitzpatrick et al., 2001). At resting membrane potential, NMDA receptors have a voltage dependent block by a magnesium (Mg^{2+}) ion tightly bound in its pore that prevents ion conductance (Mayer et al., 1984; Nowak et al., 1984; Grienberger and Konnerth 2012). When glutamate binds, AMPA receptors become activated leading to neuronal depolarization of the postsynaptic neuron. The depolarization causes the Mg^{2+} ion to be displaced from the NMDA pore, allowing monovalent ions such as Na^{+}, K^{+} and divalent Ca^{2+} ions to flow into the neuron from the extracellular environment, resulting in an even larger neuronal depolarization (Purves, Augustine, Fitzpatrick et al., 2001). Finally, kainate receptors act similarly to AMPA receptors to yield fast EPSPs in contrast to NMDA receptors which produce slower, more long-lasting EPSPs (Purves, Augustine, Fitzpatrick et al., 2001).

Metabotropic glutamate receptors are G-protein coupled receptors that modulate Ca^{2+} release and neuronal excitability by activating second messenger signalling cascades and are grouped based on their downstream signalling mechanisms (Lüscher and Huber, 2010; Niswender and Conn, 2010). For example, activation of group 1 metabotropic glutamate receptors, such as mGlu1, leads to phospholipase C hydrolyzing $PI[4,5]P_2$ into DAG and IP_3 causing the release from internal Ca^{2+} stores from the ER (Niswender and Conn, 2010). These cascades can result in a much larger release of Ca^{2+} from intracellular stores and subsequently a larger depolarization of the neuron. In contrast, Group II and III metabotropic glutamate receptors are coupled to inhibitory G-proteins and cause suppression of neuronal activity (Niswender and Conn, 2010).

1.3. Tools for Visualizing Cellular Calcium Dynamics

When Ca^{2+} is not tightly regulated it can lead to cellular dysfunction that can trigger pathogenic states and cell death pathways. Therefore, being able to visualize cellular function is very important when trying to understand both normal and pathogenic states. There are a number of tools that scientists use to study Ca^{2+} dynamics, including chemical Ca^{2+} indicators and genetically encoded Ca^{2+} indicators.

1.3.1. Chemical Calcium Indicators

Ca^{2+} cations can be held in the cytosol by Ca^{2+} buffers that are responsible for Ca^{2+} clearance, controlling the duration of Ca^{2+} signalling, and can also act as sensors. Some of these buffers include calbindin, parvalbumin and calretinin (Schwaller, 2010). Although Ca^{2+} can be bound to buffers in the cytosol, a small quantity also exists in free form at a ratio of 100:1 (bound:unbound, respectively; Paredes et al., 2008). Ca^{2+} indicators bind and interact with these free Ca^{2+} ions, acting in a similar manner to Ca^{2+} buffers. Chemical Ca^{2+} indicators are molecules that have been engineered to visualize Ca^{2+} dynamics and have both a Ca^{2+} chelating site (EGTA or BAPTA) and a fluorophore (Tsien 1980; Grynkiewicz et al., 1985; Pardes et al., 2008). Once they bind Ca^{2+} ions, there is a conformational change resulting in emission of fluorescence. Unlike other types of Ca^{2+} indicators, chemical Ca^{2+} indicators are typically loaded into cells with membrane disrupting techniques such as electroporation, microinjection or diffusion throughout the neuron with patch clamping techniques (Pardes et al., 2008).

Numerous chemical Ca^{2+} indicators have been created based on their differing affinities for Ca^{2+}, although the two most commonly used for measuring cytoplasmic Ca^{2+} levels in Ca^{2+} imaging studies are fluo-4 and fura-2. Fluo-4 is a single wavelength dye,

i.e., it is excited at one peak wavelength (488 nm excitation), causing emission at another wavelength (516 nm; Gee et al., 2000). Single wavelength dyes are advantageous in that they do not overlap with the wavelengths of other fluorophores and they are able to show large changes in fluorescence upon interacting with Ca^{2+} without any shifts in their excitation or emission wavelengths. Fluo-4 has been a popular and widely used chemical indicator because it has low background absorbance and is much brighter than other chemical indicators, thereby requiring a lower concentration of dye for experiments (Pardes et al., 2008). In contrast, fura-2 (Grynkiewicz et al., 1985) is a ratiometric indicator and is considered to be a standard for quantitative $[Ca^{2+}]_i$ measurements. Ratiometric indicators quantify Ca^{2+} flux or change in fluorescence as a ratio of the emission between two different excitation wavelengths. In the case of fura-2, the excitation peak is at 380 nm when it is not bound to Ca^{2+}, but upon binding Ca^{2+}, it shifts to 340 nm. Ratiometric indicators allow for corrections of various experimental artifacts such as uneven dye loading, photobleaching, and changes in cell volume (cell swelling; Paredes et al., 2008).

1.3.2. Genetically Encoded Calcium Indicators

As the field of Ca^{2+} imaging progressed, the need for developing methods to express Ca^{2+} indicators without having to electroporate retinas or cells became very important. This was one of the main driving forces for the creation of genetically encoded Ca^{2+} indicators (GECIs). GECIs share similar properties with chemical Ca^{2+} indicators because they also have a Ca^{2+} binding domain tagged to a fluorescent molecule, causing increases in fluorescence upon interacting with and binding Ca^{2+} ions. They also can be non-ratiometric or ratiometric depending on whether they have one or two fluorescent

proteins, respectively (Koldenkova and Nagai, 2013). The invention of GECIs occurred following three major findings: the discovery of green fluorescent protein (GFP), coloured variants, and experiments that lead to a greater understanding of how Ca^{2+} binds to calmodulin through an M13 peptide from myosin light chain kinase (Porumb et al., 1996; Koldenkova and Nagai, 2013).

The first used GECIs were termed "cameleons" and were used in fluorescence (Förster) resonance energy transfer (FRET) microscopy experiments (Miyawaki et al., 1997). FRET is a phenomenon that describes the physical transfer of energy from a donor fluorescent molecule to an acceptor and as such, is thought to be a way of measuring the distance between these donor and acceptor molecules (Sekar and Periasamy, 2003). FRET is a distance dependent process as the energy transfer is sensitive to 1-10 nm between fluorophores (Jares-Erijman and Jovin, 2003).

Cameleon GECIs are dependent on two fluorescent proteins acting together to emit fluorescence in the presence of Ca^{2+} and are therefore considered ratiometric in nature. Cameleons have a linear structure, consisting of a blue fluorescent protein (BFP; acts as the FRET donor), an M13 domain of myosin light chain kinase, calmodulin, and a GFP molecule (acts as the FRET acceptor; Miyawaki et al., 1997). When there is no Ca^{2+} bound and cameleon is excited at 370nm, the molecule remains in this linear form and no energy transfer occurs yielding no FRET signal. When cameleon binds free Ca^{2+}, there is a conformational change that brings the BFP and GFP in close proximity so that FRET can occur, passing energy from the BFP molecule to the GFP and emitting fluorescence at 510 nm, thereby increasing the FRET signal that can be visualized (Miyawaki et al., 1997; Whitaker, 2010).

The cameleon GECIs were foundational in creating the next family of GECIs, the GCaMP family. Unlike their predecessors that depended on FRET, the GCaMP family are single-fluorescent protein Ca^{2+} sensors that depend only on the excitation of one fluorescent molecule to generate one emission signal. GCaMP is composed of a circularly permutated GFP, fused to both a calmodulin and an M13 peptide at its C- and N-terminus, respectively (Nakai et al., 2001). In the absence of Ca^{2+}, the M13 peptide and calmodulin are not associated, and GCaMP emits low fluorescence (excitation 488 nm, emission 516 nm). When Ca^{2+} is present, it binds to calmodulin causing a conformational change so that the M13 peptide and calmodulin associate, resulting in an increase in the fluorescence emitted. Since they emit fluorescence at only one single wavelength, they are considered non-ratiometric (Koldenkova and Nagai, 2012).

The GCaMP family is constantly evolving, with different variants being created based on their fluorescent and kinetic properties as well as their Ca^{2+} binding affinities. For a long time, GCaMP3 was the most popular variant used in detecting neuronal activity in the cortex, hippocampus, and retina, as it was superior to previous variants (GCaMP and GCaMP2) because of its increased affinity for Ca^{2+}, increased baseline fluorescence, and larger dynamic range (Tian et al., 2009). Since then, more GCaMP variants have been created, each attempting to improve on those three characteristics. The GCaMP6 family has become widely used in brain and retina research for *in vivo* Ca^{2+} imaging (Chen et al., 2013; Bar-Noam, Farah and Shoham, 2016; Ye et al., 2017; Cheong et al., 2018a; Cheong et al., 2018b). The GCaMP6 family is comprised of GCaMP6s, GCaMP6m, and GCaMP6f, named based on their rise and decay kinetics (slow, medium and fast, respectively; Chen et al., 2014). The GCaMP6 family all exhibit lower baseline

fluorescence, higher affinity for Ca^{2+} than GCaMP3, and an improved signal-to-noise ratio, allowing more accurate and sensitive measures of neuronal Ca^{2+} dynamics.

There has also been progress in the creation of different color variants, such as the red-shifted variants, R-GECO (Zhao et al., 2011; Broussard et al., 2014). The GCaMP family is a green fluorescent indicator and is excited at a shorter wavelength than red-shifted indicators. Shorter wavelength light can be more phototoxic than longer wavelength light (Ham et al., 1976), so the red shifted GECI, jRGECO1a, has been introduced to the field as an alternative and a potentially less phototoxic tool as the use of *in vivo* functional imaging increases.

There are a number of advantages of GECIs over chemical Ca^{2+} indicators. They can be expressed in a specific population of cells using promoter sequences that are cell-type specific. The creation of GECIs provided the impetus for the introduction of various strains of transgenic mice. The use of these mice allows for a more convenient way to express GECIs for performing longitudinal experiments, and for *in vivo* experiments to be performed without having to introduce the exogenous fluorophore with invasive procedures.

1.3.3. The Thy1-GCaMP3 Transgenic Mouse Strain

Because mice can be genetically manipulated to express, or not to express, selected genes and proteins, they are valuable in many disease models. In 2012, Chen and colleagues created the first transgenic mouse strain that expressed GCaMP3 under the control of a Thymocyte differentiation antigen 1 (Thy1) promoter. They started with six founder lines that varied in levels and patterns of GCaMP3 expression in excitatory projection neurons. They used the six lines to breed the mice at an expected Mendelian

rate and found that GCaMP3 was expressed in a widespread fashion throughout the CNS. GCaMP expressed in the neurons in this transgenic mouse strain was found in the somata and neurites, but not in the nucleus (Chen et al., 2012). The Thy1-GCaMP3 mice also showed no histological or behavioural abnormalities.

Although the majority of experiments using the Thy1-GCaMP3 transgenic mouse strain have been performed in brain, characterization the GCaMP3 expression in the retina has also been performed, specifically for *ex vivo* Ca^{2+} imaging experiments in RGCs. It was found that GCaMP3 was widely and uniformly expressed across central, middle and peripheral retina and that the expression was primarily localized to the GCL, with some displaced RGCs in the INL showing GCaMP3 expression. When specificity studies with immunohistochemistry (IHC) were performed, the GCaMP3 (labelled with GFP to amplify the fluorescence signal) colocalized primarily with RGCs and rarely with displaced amacrine cells (Blandford et al., 2019).

The functional responses of the GCaMP3 in RGCs have also been characterized in brain (Chen et al., 2012), and recently in retina (Blandford et al., 2019). It has been found with Ca^{2+} imaging, that kainic acid (KA)-induced Ca^{2+} transients can be evoked in RGCs in a dose-dependent manner. Blandford and colleagues also reported Ca^{2+} responses following optic nerve transection (ONT); a procedure where the optic nerve is completely severed, leading to rapid cell death and loss of RGCs (Quigley et al., 1977; Berkelaar et al., 1994). They were able to show a significant decrease and eventual complete loss of KA-induced transients as early as three days post-ONT. Although there were visible cells with Ca^{2+} imaging at five- and seven-days post-ONT, they were not responsive to KA treatments, indicating that functional loss precedes structural loss (Blandford et al., 2019).

1.4. Adeno-Associated Viral Vectors as a Tool to Deliver Structural and Functional Markers

Transgenic mice such as the Thy1-GCaMP3 and Thy1-GCaMP6 mouse strains that express GECIs have and continue to be a valuable resource that have allowed for the expansion of our knowledge of both *ex vivo* and *in vivo* Ca^{2+} dynamics. However, the major limitation remains that transgenic mice are not clinically relevant, and research cannot be directly translated for clinical use as genetic manipulation is not possible or ethical. Therefore, researchers have developed different methods to exogenously deliver proteins for gene therapy, as well as fluorescent molecules for both structural and functional fluorescent imaging in the retina. With the exception of photoreceptors that can be imaged with adaptive optics because of their high refractive index, the ability to visualize retinal cells that would otherwise be transparent is an invaluable tool.

The most commonly used method for delivery into the retina is the use of viral vectors, more specifically adeno-associated viral (AAV) vectors. AAV is a single stranded DNA virus in a non-enveloped icosahedral capsid. It is a small virus, approximately 25 nm in size, from the *Parvoviridae* family with a genome consisting of approximately 4.7 kb (Balakrishnan and Jayandharan, 2014; Colella, Ronzitti and Mingozzi, 2018). It is primarily episomal, therefore, it does not integrate into the cell genome. AAV is non-pathogenic and is able to provide long transgene expression in infected cells, making it a highly attractive choice for gene therapy and delivery (Zincarelli et al., 2008).

There are a number of AAV serotypes which are differentiated by the surface antigens they express on their capsid and some serotypes have been found to be preferable for viral transduction in different tissues. For example, AAV8 has been shown

to have the highest level of transgene expression in the liver in comparison to other serotypes (Gao et al., 2002), while AAV2 and AAV9 have been shown to have high levels of transgene expression in the CNS, notably in the retina (Lei et al., 2009; Lee et al., 2019). A recent study showed that labelling with AAV9 in retina can be weak or patchy in comparison to AAV2 which was more robust and widespread, leaving AAV2 as potentially more preferable for labelling RGCs in mice (Cheong et al., 2018a).

AAV vectors have been used to deliver therapeutic agents, structural and functional makers to the retina (for reviews see: Hauswirth, 2014; Pierce and Bennett, 2015). There are three main routes of administration, via injection, to the retina: suprachoroidal, subretinal and intravitreal. Suprachoroidal injections primarily target the choroid, RPE and outer retinal neurons, as the virus is injected into the suprachoroidal space, the space between the choroid and the sclera. Subretinal injections target cells that reside in the outer retina (namely RPE cells and photoreceptors) because the viral vector is injected in the potential space between the RPE and the photoreceptor layer of the outer retina (Ochakovski et al., 2017). In contrast, intravitreal injections are preferable for targeting the inner retina (RGCs and amacrine cells). With intravitreal injections, the vector is injected directly into the vitreous humour, the fluid that fills the posterior chamber of the eye. It is a minimally invasive technique and is widely used clinically to deliver agents to the retina.

AAV has been used to deliver structural markers such as GFP to the inner retina. It has been used to quantify cells transduced by the virus and monitor cell structure before and after inducing an injury in a number of different animal models. For example, in non-human primates (NHP) such as the macaque monkey, it has been shown that AAV2-GFP labelling is relatively concentrated to the foveal region of the retina (Yin et al., 2011; Yin

et al. 2014). In New World marmosets, another NHP, when CAG (cytomegalovirus (CMV) early enhancer/chicken β actin) or CMV (cytomegalovirus) promoters were used, more widespread labelling of GFP was found across the retina (Ivanova et al., 2010). Smith and Chauhan demonstrated *in vivo* longitudinal imaging and tracked the transduction of cells labelled with both a specific (DCX; doublecortin) and ubiquitous (CAG) promoter over time in wild type mice using AAV2. They were also able to report a decrease in the number of cells labelled with the AAV2 vector *in vivo* following ONT and co-localized those lost cells to baseline images (Smith and Chauhan, 2019).

Although this technique allows retinal cells to be labelled with a structural marker, it does not allow for the inference or knowledge of their functional status. Therefore, in recent years, several groups have reported delivery of GECIs, such as GCaMP to the retina to obtain functional responses from RGCs by using AAV (Borghuis et al., 2011; Sharma et al., 2013; Weitz et al., 2013) and rabies virus (Yin et al., 2013). GCaMP3 transduced by AAV has been shown to be functional with *ex vivo* Ca^{2+} imaging with pulse stimulation through an electrode (Borghuis et al., 2011; Weitz et al., 2013) and is actively used as a tool to visualize Ca^{2+} dynamics *in vivo* using two-photon (2P) and multi-photon microscopy in rodent models.

In a number of *in vivo* 2P dynamic imaging experiments, GCaMP3 has been used as a structural marker because of its high baseline fluorescence, however, due to its small dynamic range, other members of the GCaMP family have been used for functional experiments. GCaMP6s has been used for successfully recording *in vivo* functional data from RGCs with optical stimuli (Bar Noam et al., 2015, Cheong et al., 2018a; Qin et al., 2020). There has also been an increase in the use of red-shifted Ca^{2+} GECIs in monitoring

cellular function in the retina such as jRGECO1a as it has been found to provide similar results to GCaMP6s (Chen et al., 2013; Cheong et al., 2018b).

1.5. Objectives and Hypothesis

Previous research on RGC functional responses in the transgenic Thy1-GCaMP3 mouse strain has been reported (Blandford et al., 2019); however, delivery of GECIs exogenously is a more rational approach for clinical translation. In our laboratory, there has been recent work demonstrating the delivery of structural markers to the retina and the ability to monitor that fluorescence over time (Smith and Chauhan, 2018). However, we know from *ex vivo* studies that neuronal dysfunction precedes structural changes in RGCs (Blandford et al., 2019). Therefore, the overarching goal of this research was to label RGCs with an exogenous functional fluorescent marker and to be able to visualize these cells with longitudinal *in vivo* imaging. Using intravitreal injection, my project sought to characterize the AAV2-CAG-GCaMP3 viral vector as a tool to accomplish functional imaging.

The objectives of this thesis were to:

1. Track the transduction of retinal cells labelled with AAV2-CAG-GCaMP3 using longitudinal *in vivo* imaging.
2. Evaluate the functional properties of the AAV2-CAG-GCaMP3 viral vector transduced in retinal cells and compare that to those of the Thy1-GCaMP3 transgenic mouse strain.
3. Examine the specificity of the AAV2-CAG-GCaMP3 viral vector to cells residing in the GCL.

We hypothesized that the viral vector could be successfully transduced in RGCs and that the transduced GCaMP3 protein would yield a viable functional signal upon chemical stimulation.

CHAPTER 2. Materials and Methods

2.1. Animals

Animal procedures were conducted in accordance with the Canadian Council of Animal Care (CCAC) and the Animal Ethics Committee at Dalhousie University. Adult female C57Bl/6 mice (JAX^{TM} Mice Stock Number: 000664, Charles River Laboratories, Saint-Constant, QC, Canada) were used in this study. The mice were housed in an environment with a 12-hour light-dark cycle and access to food and water *ad libitum*. Twelve mice were used to quantify the transduction of the AAV2-CAG-GCaMP3 virus with longitudinal *in vivo* imaging over five weeks, 10 mice were used for *ex vivo* Ca^{2+} imaging in both the Thy1-GCaMP3 transgenic mouse group and the AAV injected group, and six retinas from mice injected with AAV2-CAG-GCaMP3 were used for IHC. For both the *in vivo* imaging sessions and the intravitreal injection procedures, mice were anesthetized with 2% isoflurane (Baxter Corporation, Mississauga, ON, Canada) and 1% O_2 administered at a flow rate of 1.5 L/min via a nose cone.

The GCaMP3 vector was chosen for this work for two reasons: the first being that GCaMP3 has point mutations allowing it to emit brighter baseline fluorescence than previous GCaMP variants (Tian et al., 2009) making it optimal for visualizing transduced cells with longitudinal *in vivo* imaging. Secondly, we chose to deliver GCaMP3 to ensure that we make direct comparisons to the Thy1-GCaMP3 transgenic mouse strain during *ex vivo* experiments.

2.2. Intravitreal Injection

All mice used in the study, with the exception of the transgenic mice used for Ca^{2+} imaging, received an intravitreal injection of AAV2-CAG-GCaMP3 (Vigene Biosciences, Inc., Rockville, MD). For this procedure, the left pupil was first dilated with 1% tropicamide (Alcon, Mississauga, ON, Canada) and 2.5% phenylephrine hydrochloride (Alcon). The mice were anesthetized, and a 30G needle was used to create a puncture in the sclera, 0.5 mm posterior to the limbus. The tip of a 33G needle (Hamilton Company, Reno, NV, USA) was guided through the puncture site and 1.5 µL of the AAV2-CAG-GCaMP3 viral vector at a titer of $1x10^{13}$ vg μl^{-1} was injected posterior to the lens, into the vitreous. Following the injection, topical antibacterial eye drops were administered, and the animals recovered on a heating pad overnight.

2.3. In Vivo Longitudinal Imaging

Prior to *in vivo* imaging, the left pupil was dilated with 1% tropicamide (Alcon, Mississauga, ON, Canada) and 2.5% phenylephrine hydrochloride (Alcon). Mice were anesthetized and a polymethyl methacrylate contact lens (Cantor and Nissel Limited, Brackley, UK) was placed on the cornea to maintain hydration of the cornea (thereby preventing cataracts and corneal ulcerations) and enhance image quality. A confocal fluorescence scanning laser ophthalmoscope (CSLO)/spectral-domain optical coherence tomography (OCT) device modified for use in mice (Spectralis Multiline, Heidelberg Engineering GmbH, Heidelberg, Germany) was used for the *in vivo* imaging (Chauhan et al., 2012).

With the CLSO centered on the optic nerve head and focused on the nerve fiber layer, virus transduced, fluorescently labelled retinal cells within a 30° field of view were

imaged. The CSLO software minimizes motion artefacts from respiration by using real-time eye tracking (Chauhan et al., 2012). The software also registers all follow-up images to baseline such that an accurate serial analysis in exactly corresponding locations can be performed. Fluorescence images were acquired with 488 nm excitation and emission bandpass filter of 500-550 nm (Chauhan et al., 2012).

Baseline images were acquired with infrared light (IR; 820 nm) prior to the intravitreal injection. Following the intravitreal injection, mice were imaged weekly for five weeks before being sacrificed for either *ex vivo* Ca^{2+} imaging or immunohistochemistry. At each timepoint, IR images, fluorescence images, circle scans and B scans were acquired. The latter two scans allow for visualization of the retina in cross section and were acquired to monitor retinal integrity over the time-course of the experiment.

2.4. Calcium Imaging

After five weeks of monitoring transduction of retinal cells with AAV2-CAG-GCaMP3 by *in vivo* imaging, a subset of mice were sacrificed with an overdose intraperitoneal injection of sodium pentobarbital. Retinas were dissected and mounted on filter paper before being submerged in oxygenated Hanks Balanced Salts Solution (HBSS; 100% O_2, 1 mM HEPES; Praxair, Dartmouth, NS) at a pH of 7.4 and placed in a microscope mounted superfusion chamber. The retinas were perfused at a rate of 2 mL/minute for the duration of the Ca^{2+} imaging experiments.

The retinas were imaged with a 40X water immersion objective (0.80W numerical aperture, Achroplan; Carl Zeiss Meditec, Oberkochen, Germany) that was connected to a charge-coupled device camera (Sensicam PCO, Kelheim, Germany). All experiments

were recorded with this system using Axon Imaging Workbench 4 software (Molecular Devices, Sunnyvale, CA, USA). Once the tissue was placed in the superfusion chamber, the microscope was focused on the GCL and the experiments began with five minutes of baseline imaging at an acquisition rate of one frame per 20 seconds. The GCaMP3 fluorescence in both the transgenic and virus injected mice was stimulated with 488 nm excitation and collected at 516 nm emission. Following five minutes of baseline imaging, 30 second baths of 50 μM KA dissolved in 100% oxygenated HBSS were performed followed by 15 minutes of washout in the oxygenated HBSS solution between each KA treatment. 50 μM KA was chosen from previously published literature because it was sufficient to evoke transients in the majority of cells without causing signal saturation. Each retina was treated four times with KA. During each KA treatment, images were acquired at a rate of one frame per five seconds and during the washout periods, images were acquired at one frame per 20 seconds.

2.5. Immunohistochemistry and Tissue Preparation

Following five weeks of viral transduction, mice that were not used for Ca^{2+} imaging were sacrificed, and retinas were dissected and prepared for IHC. Dissected retinas were fixed at room temperature in 4% paraformaldehyde (PFA) for one hour. Following one hour of fixation, retinas were washed with phosphate buffered saline (PBS) and blocked in 10% normal donkey serum (Jackson ImmunoResearch Laboratories Inc., West Grove, PA, USA) in PBS with 0.3% Triton X-100 overnight at 4°C. Retinas were left to incubate in primary antibodies against RNA-binding protein with multiple splicing (RBPMS; 1:1000 guinea pig anti-RBPMS, PhosphoSolutions #1832, Aurora, Colorado, USA) and choline acetyltransferase (ChAT; 1:100 goat anti-ChAT,

PhosphoSolutions #315, Aurora, CO, USA) for five days at 4°C to stain for RGCs and cholinergic amacrine cells, respectively. Retinas were washed in PBS and incubated in secondary antibodies; Cy3 (1:1000 Cy3 conjugated donkey anti-guinea pig, Jackson Immuno Research Laboratories Inc., West Grove, PA, USA), Alexa Fluor® 633 (1:1000 Alexa Fluor® 633 conjugated donkey anti-goat, Invitrogen #A21082) and Alexa Fluor® 488 (1:100 Alexa Fluor® 488 conjugated antibody, Invitrogen #I21411, Carlsbad, California, USA) overnight. Alexa Fluor® 488 was used to enhance the GFP signal from the GCaMP. The following day, retinas were washed in PBS, mounted on microscope slides with Vectashield® anti-fade fluorescent mounting medium (Vector Labs, Burlingame, CA) and cover-slipped in preparation for epifluorescence imaging.

2.6. Ex vivo Epifluorescence Imaging and Image Processing

Tiled images of retinal wholemounts were obtained using a Zeiss Axio Imager M2 microscope (Carl Zeiss AG, Oberkochen, Germany) with a 20x Plan-Apochromat objective (0.8 numerical aperture; Carl Zeiss). Using Zen Software (Carl Zeiss), exposure times were set for each of the three channels and fluorescence images of cells expressing GFP (GCaMP), RBPMS and ChAT in the GCL were acquired.

2.7. Data Analysis and Statistics

Statistics were performed using Prism (version 8 for Macintosh, GraphPad Software, La Jolla, CA, USA) and statistical significance was assumed when $p < 0.05$.

2.7.1. In Vivo Imaging

In vivo images acquired weekly with the CSLO were imported into image J. Using the cell counting tool, the labelled fluorescent cells were manually counted. The total number of cells was divided by the retinal area which excluded the optic nerve head and large vessels and reported as a cell density (cells/mm^2). A repeated measures one-way ANOVA was performed with Tukey's multiple comparisons test to compare the difference between pairs of means with appropriate adjustment for multiple testing.

2.7.2. Calcium Imaging

Experiments were recorded and analyzed using Axon Imaging Workbench 4 (Molecular Devices, Sunnyvale, CA, USA). Focussing on the GCL, cells expressing the virus were traced as individual regions of interest (ROI). For each experiment, 40-50 cells were selected and tracked for the duration of the experiment. Baseline fluorescence for each cell was measured from the first 15 frames of the recorded experiment where the retina was bathed in oxygenated HBSS. Maximum fluorescence was determined for each cell for each of the KA treatments. KA-induced Ca^{2+} transient amplitudes were defined as the peak fluorescence change over the baseline fluorescence ($\Delta F/F_0$). A one-way ANOVA was performed for each group to determine if there were any statistically significant differences over the four KA treatments. T-tests were performed to determine any significant differences between virus and transgenic mouse groups at each KA treatment.

2.7.3. Immunohistochemistry

The image analysis for the wholemounted retinas was performed using Zen2Lite software (Carl Zeiss Meditec, Oberkochen, Germany). From the tiled image of the wholemounted retinas, 500 µm x 500 µm ROIs were selected. In each quadrant, ROIs were selected from central, middle and peripheral retina to yield 12, 500 µm x 500 µm, ROIs per retina. For each ROI, cell counts were performed for the each of the three channels individually; GFP (GCaMP), RBPMS, and ChAT as well as the GFP-positive cells that colocalized with RBPMS-positive cells, and ChAT-positive cells. The cell counts were expressed as mean densities (standard deviation). One-way ANOVAs were performed for each channel to determine statistical significance between cell densities across central, middle and peripheral retina.

CHAPTER 3. Results

3.1. Quantification of the Transduction of AAV2-CAG-GCaMP3 in Retinal Cells

The GCaMP3 transduced by the virus was visible with CSLO in the GCL one-week following intravitreal injection, and the expression increased steadily every week for five weeks (Figure 3.1). The labelling was visualized in the somata and axons of retinal cells. In the majority of mice, the labelling was more intense, and the fluorescence was brighter in the superior-temporal portion of the retina, as that was the proximal site of the injection. The labelling spread from this region across the retina over the course of five weeks. Furthermore, in the majority of mice injected with the virus, the fluorescence intensity was weak one-week post-injection and was increased by two-weeks post-injection.

When quantified, the mean (standard deviation) cell density one-week post-injection was 191 (39) cells/mm^2 and this increased to 586 (67) cells/mm^2 at five weeks post-injection (Figure 3.2). A repeated measures one-way ANOVA was performed and indicated a significant increase in the density of labelled cells each week (weekly from baseline to week 4: $p < 0.0001$, week 4 to week 5: $p < 0.001$). In a mouse that was followed over a longer time-course, the labelling and expression of the transduced GCaMP3 persisted for six months post-injection (Figure 3.3). With monthly imaging sessions, the cellular labelling remained consistent and the vitreous remained clear in this mouse, allowing for the registration of all follow-up images to baseline over the six-month time-course.

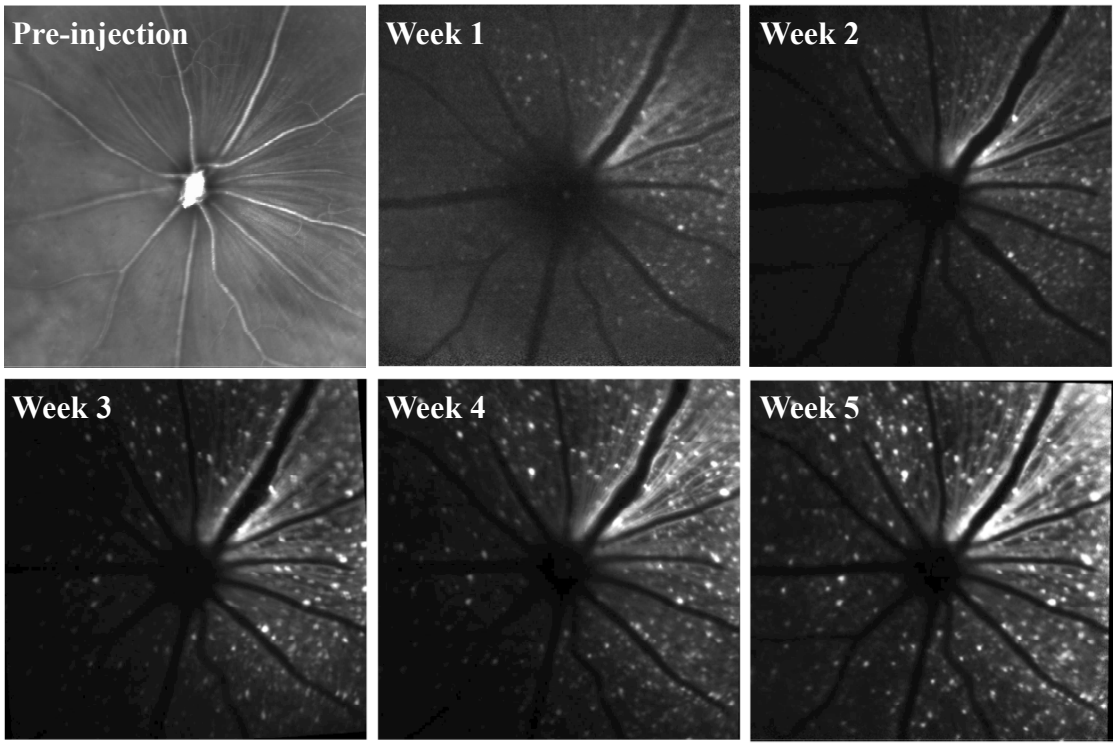

Figure 3.1. Longitudinal *in vivo* imaging of a mouse injected with AAV2-CAG-GCaMP3 over five weeks. One representative mouse injected with AAV2-CAG-GCaMP3 imaged weekly over five weeks. A baseline IR image was acquired prior to the injection. Week-one through week-five fluorescence images were taken post-injection with image registered acquisition.

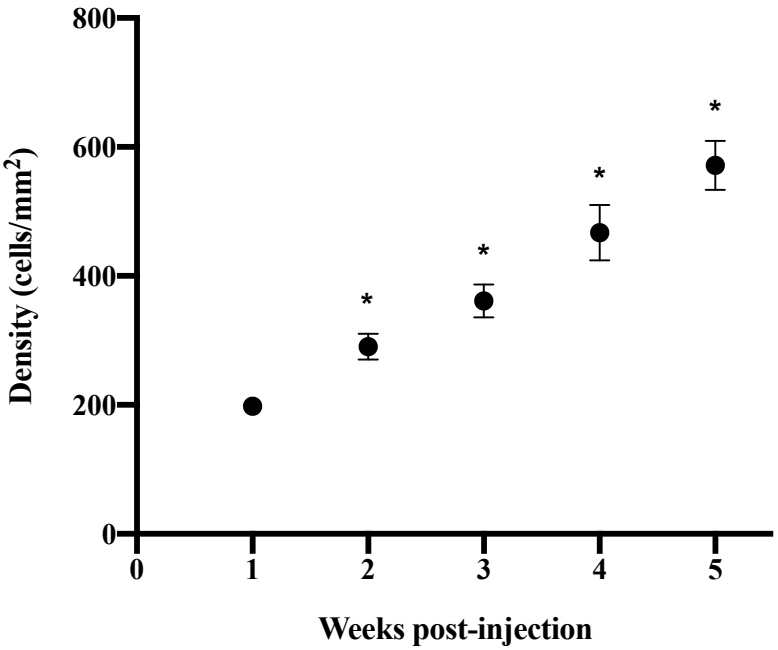

3.2. *In vivo* quantification of the transduced GCaMP3 expressed in retinal cells in the ganglion cell layer following intravitreal injection. At each timepoint, cell densities were calculated from the *in vivo* images. Repeated measures one-way ANOVA with Tukey's multiple comparisons test confirmed significance of $p < 0.05$ each week; n=12. Mean (SD) are reported.

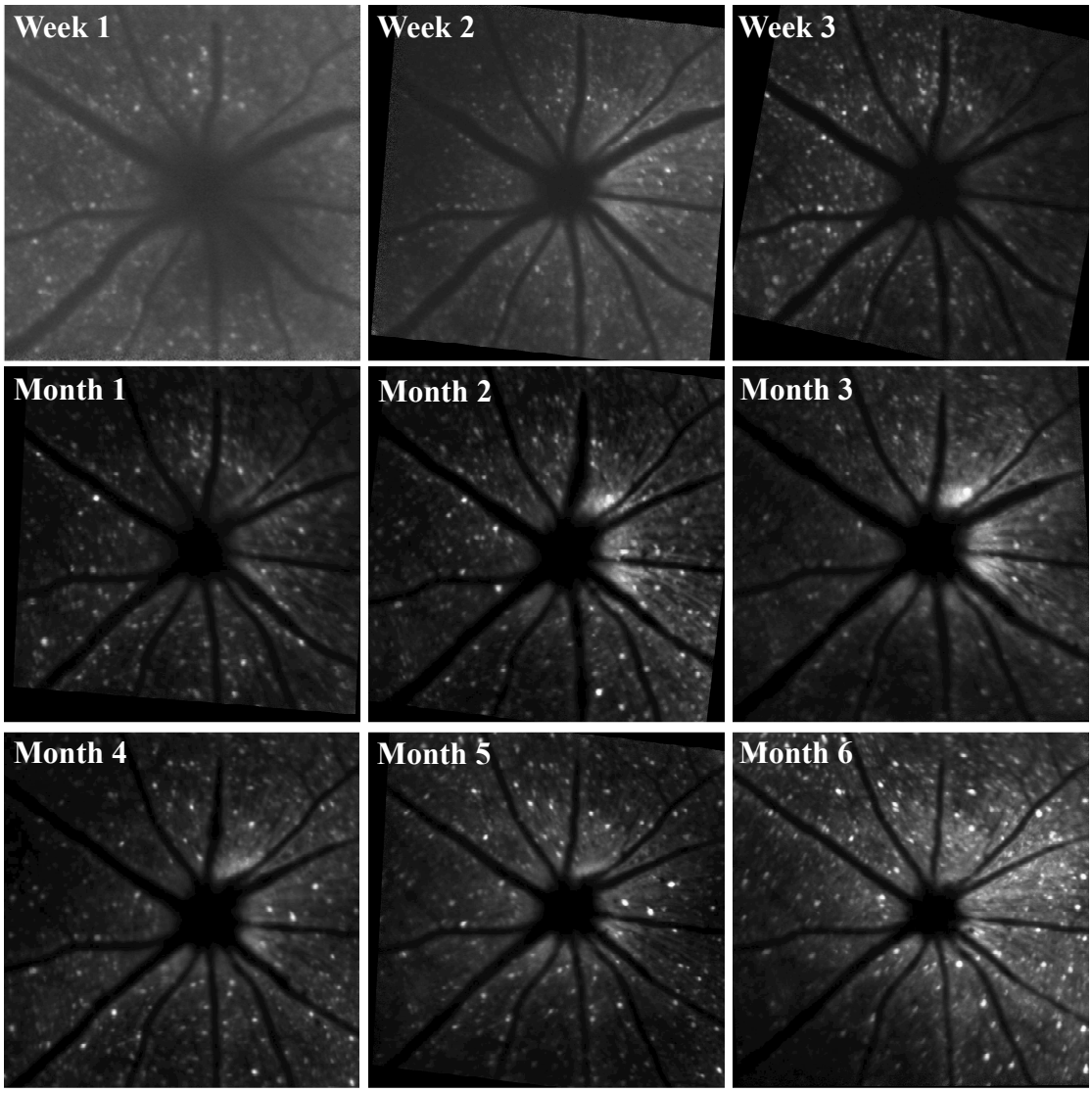

Figure 3.3. Longitudinal *in vivo* imaging of a mouse injected with AAV2-CAG-GCaMP3 over six months. Images acquired from the same mouse injected with AAV2-CAG-GCaMP3 demonstrating that labelling persists to six months following injection. The mouse was imaged weekly for the first month following injection and monthly until six months, each imaged was registered to baseline.

3.2. Comparison of Thy1-GCaMP3 and AAV2-CAG-GCaMP3 Transients

Isolated retinas treated with 50 µM of kainic acid (KA) successfully produced KA-induced Ca^{2+} transients, or increases in the transient amplitudes which is indicative of increases in the GCaMP fluorescence, in retinas from both Thy1-GCaMP3 transgenic mice and retinas from the AAV2-CAG-GCaMP3 injected mice (Figures 3.4 and 3.5, respectively). Following the transient increases in response to KA treatments, GCaMP3 labelled cells from both groups successfully returned to baseline levels with KA washout following each of the four treatments, which was visualized through pseudo-colour videos. Frames from the videos are shown in Figures 3.4 and 3.5 where cooler colours are indicative of lower levels of Ca^{2+} and warmer colours are indicative of higher levels of Ca^{2+}.

When groups were analyzed individually, the KA-induced Ca^{2+} transients showed no statistically significant differences between each of the four treatments of KA in either the transgenic group or the virus injected group ($p = 0.43$ and $p = 0.97$ respectively; Table 3.1), indicating that the GCaMP was consistently and reliably responding to KA treatments. Furthermore, when the two groups were compared, there were no significant differences found in the mean transient amplitudes between the Thy1-GCaMP3 retinas and retinas transduced with AAV2-CAG-GCaMP3 over any of the four treatments of KA. However, the transients recorded from GCaMP3 labelled cells in the virus injected group were more variable than those in the transgenic group (Figure 3.6; Table 3.1).

Retinas from the virus injected group also displayed regions of increased baseline fluorescence in comparison to other fields of view within the same retina. When stimulated, these regions became oversaturated and hyper-fluorescent in response to treatments of 50 µM KA, as indicted by bright red signals on the pseudocoloured video

(Figure 3.7). It is likely the increased fluorescence in these fields of view are due to these regions being near the superior-temporal region.

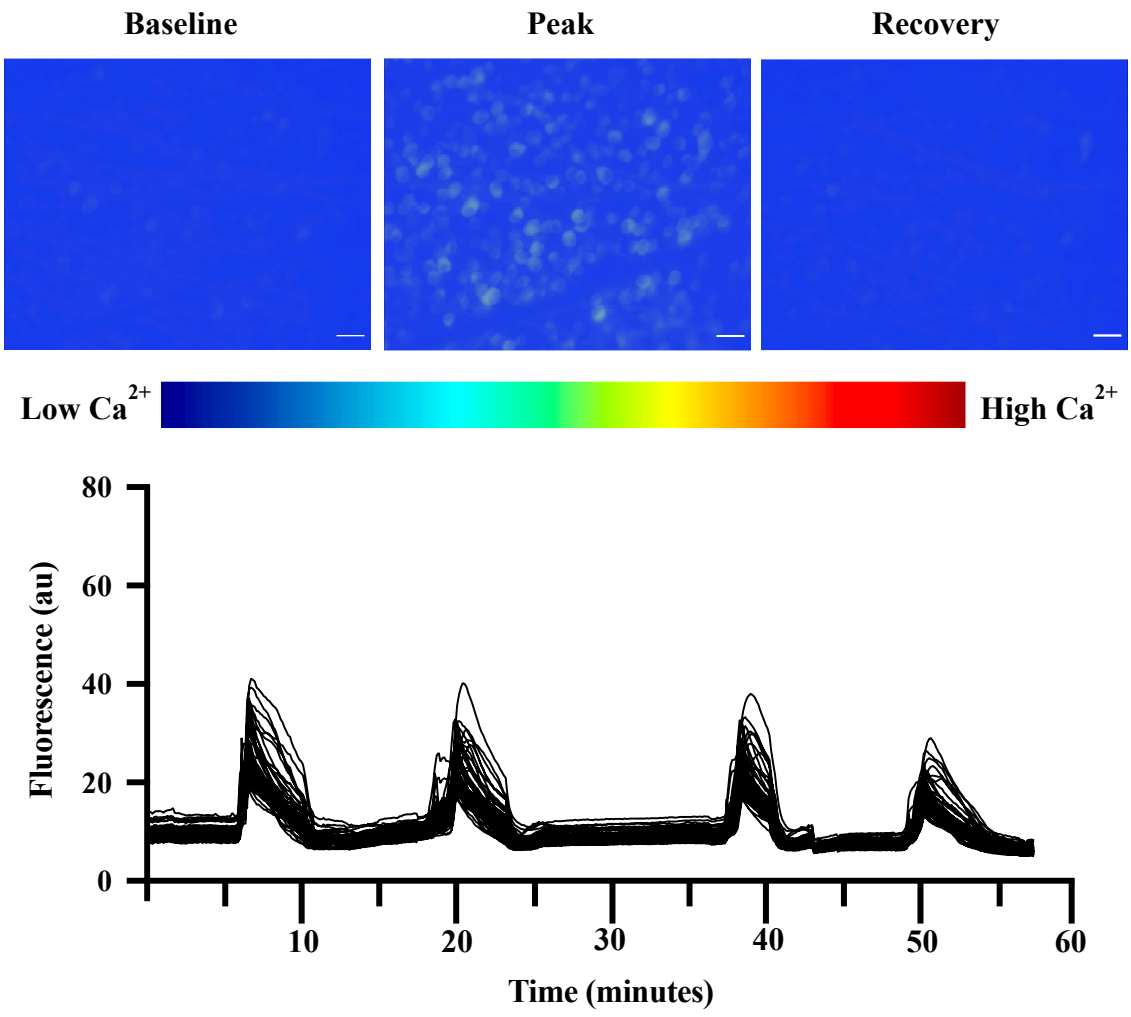

Figure 3.4. Calcium transients in a Thy1 GCaMP3 transgenic mouse.

A) Pseudocoloured images acquired from one calcium imaging experiment performed in a retina from a Thy1-GCaMP3 mouse. Images (left to right) show baseline fluorescence, the KA-induced peak in GCaMP3 fluorescence, and recovery to baseline Ca^{2+} levels upon KA wash out. Scale bars= 50 µm. (B) Example traces from 50 cells selected in the experimental field of view over four, 30-second treatments of 50 µM KA demonstrating the increases in GCaMP3 fluorescence in response to KA.

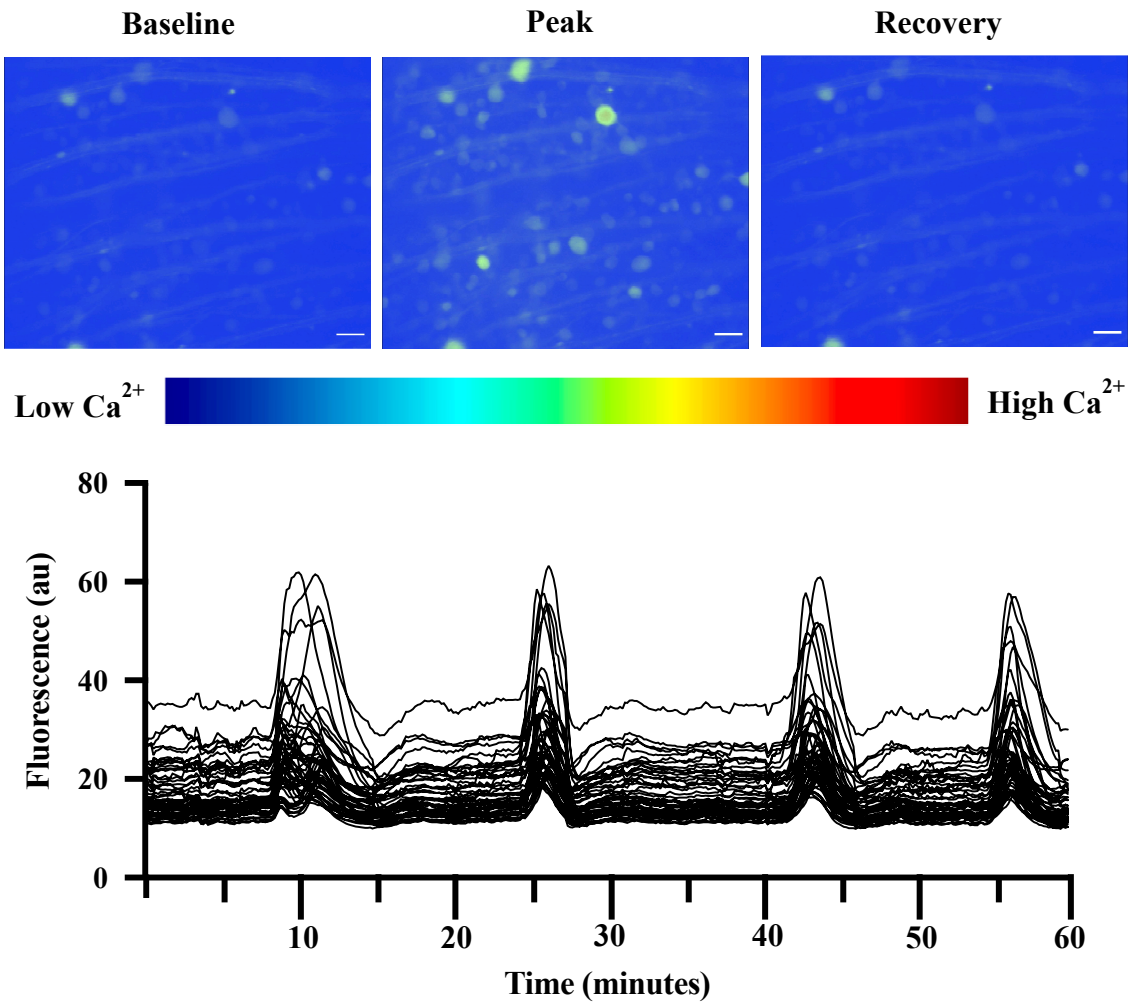

Figure 3.5. Calcium transients in a mouse injected with AAV2-CAG-GCaMP3.
A) Pseudocoloured images acquired from one calcium imaging experiment performed in a retina from a mouse injected with AAV2-CAG-GCaMP3. Images (left to right) show baseline fluorescence, the KA-induced peak in GCaMP3 fluorescence, and recovery to baseline Ca^{2+} levels upon KA wash out. Scale bars= 50 µm. (B) Example traces from 50 cells selected in the experimental field of view over four, 30-second treatments of 50 µM KA demonstrating the increases in GCaMP3 fluorescence in response to KA.

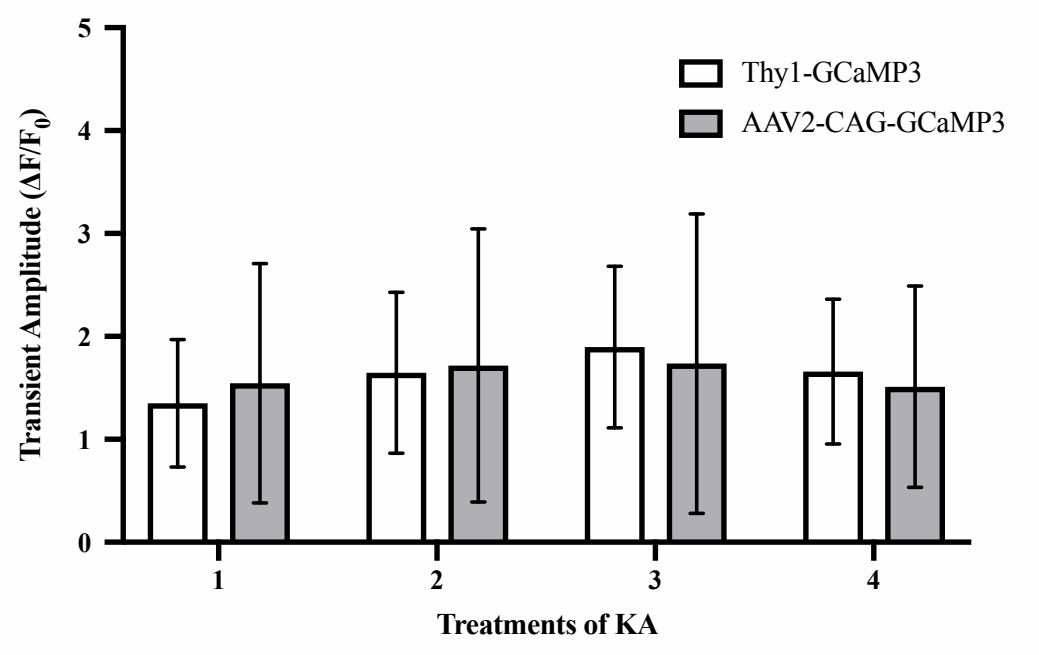

Figure 3.6. Comparison of calcium transients between the Thy1-GCaMP3 transgenic mice and the AAV2-CAG-GCaMP3 injected mice. Mean data show transient amplitudes for the Thy1-GCaMP3 and AAV2-CAG-GCaMP3 groups over four, 30-second treatments of 50 μM KA (*n* = 482 total cells from 10 experiments in the Thy1-GCaMP3 group and 474 total cells from 10 experiments in the AAV2-CAG-GCaMP3 group. Mean (SD) are reported.

Table 3.1. Comparison of the KA-induced Ca^{2+} transients in the Thy1-Transgenic and AAV2-CAG-GCaMP3 injected mice.

KA Treatment	1	2	3	4	*p*
Thy1-GCaMP3[1]	1.35 (0.62)	1.65 (0.78)	1.90 (0.79)	1.66 (0.70)	*0.43*
AAV2 -GCaMP3[2]	1.55 (1.16)	1.72 (1.33)	1.74 (1.46)	1.51 (0.98)	*0.97*

[1] n = 482 total cells from 10 experiments
[2] n = 474 total cells from 10 experiments
Data represents the mean peak fluorescence change over the baseline fluorescence ($\Delta F/F_0$). Data is reported as mean (standard deviation).

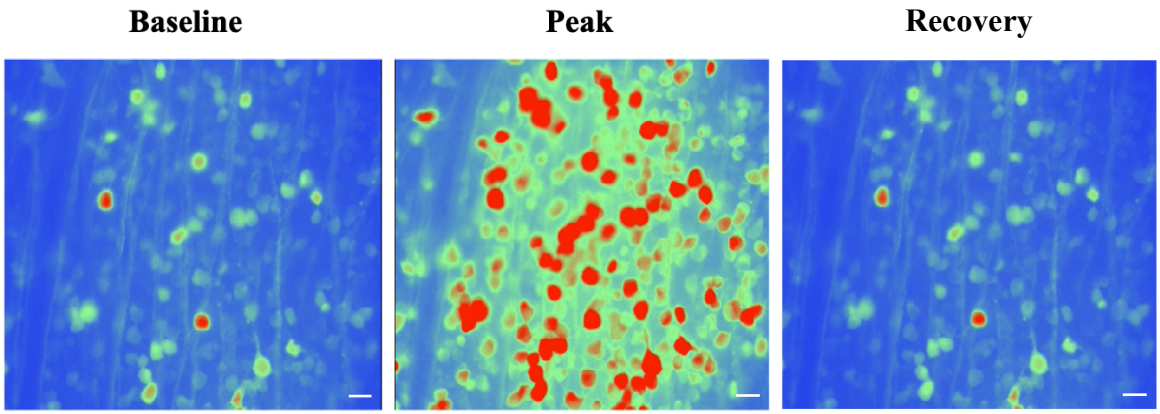

Figure 3.7. Hyper-reflective regions in a retina from a mouse injected with AAV2-CAG-GCaMP3. Pseudocoloured images acquired from a field of view in one Ca^{2+} imaging experiment performed in a retina from a mouse injected with AAV2-CAG-GCaMP3 demonstrating increased baseline fluorescence and saturation of cells following KA-treatment. Images (left to right) show baseline fluorescence, the KA-induced peak in GCaMP3 fluorescence, and recovery to baseline Ca^{2+} levels upon KA wash out. Scale bars= 50 μm.

3.3. Specificity of AAV2-CAG-GCaMP3 to Cells in the GCL

When immunohistochemistry was performed, robust GFP labelling was visualized in the GCL with epifluorescence microscopy in wholemounted retinas (Figure 3.8). Similar to observations made with *in vivo* imaging, immunohistochemistry showed intense GFP fluorescence in the superior-temporal region in comparison to other retinal regions or quadrants (Figure 3.9). Increased fluorescence in this region was visualized in retinas from every mouse injected with the virus. Although the fluorescence was increased in the superior-temporal region, there was still widespread labelling visualized and quantified across the entire retina.

Following quantification of cell densities for RBPMS, ChAT and GFP in the GCL, the average density of RBPMS-positive cells was 3086 (832) cells/mm^2, the average density of ChAT-positive cells was 1103 (189) cells/mm^2, and the average density of GFP-positive cells was 1155 (285) cells/mm^2. The GFP-positive and ChAT-positive cells were widely distributed throughout the retina with no significant differences in cellular densities between central, middle and peripheral retina ($p = 0.96$ and $p = 0.07$, respectively), indicating that in the case of GFP-positive cells, the virus was able to adequately diffuse throughout the vitreous and cross the ILM in all retinal regions. In contrast, the density of RBPMS-positive cells decreased significantly with increasing distance from the optic nerve head ($p < 0.005$, Figure 3.10), which has been previously reported (Rodriguez et al., 2014).

There was a high specificity of the viral vector for RGCs in the GCL with 79 (6)% of RBPMS-positive cells colocalizing with GFP-positive cells. In contrast, when the number of RBPMS-positive cells that were GFP-positive were analyzed, indicative of the proportion of RGCs in the retina labelled by the viral vector, it was determined that

29 (5)% were labelled (Figure 3.11). The virus also labelled cholinergic amacrine cells with 9 (4)% of GFP-positive cells colocalizing with ChAT-positive cells. There were, however, a number of GFP-positive cells quantified in the GCL that did not colocalize with either RBPMS-positive or ChAT-positive cells which made up the remaining 12 (7)% (Figure 3.12).

When epifluorescence microscopy was performed at deeper retinal layers to determine the penetrance of the vector, there was robust labelling of GFP-positive cells visualized in the INL (Figure 3.13). Although it was not quantified in each retina, there appeared to be colocalization of GFP-positive cells with ChAT-positive cells in the INL. There was also colocalization of GFP-positive with ChAT-negative cells, indicating that the GCaMP is transduced in not only cholinergic amacrine cells, but other subtypes of amacrine cells, and bipolar cells in the INL.

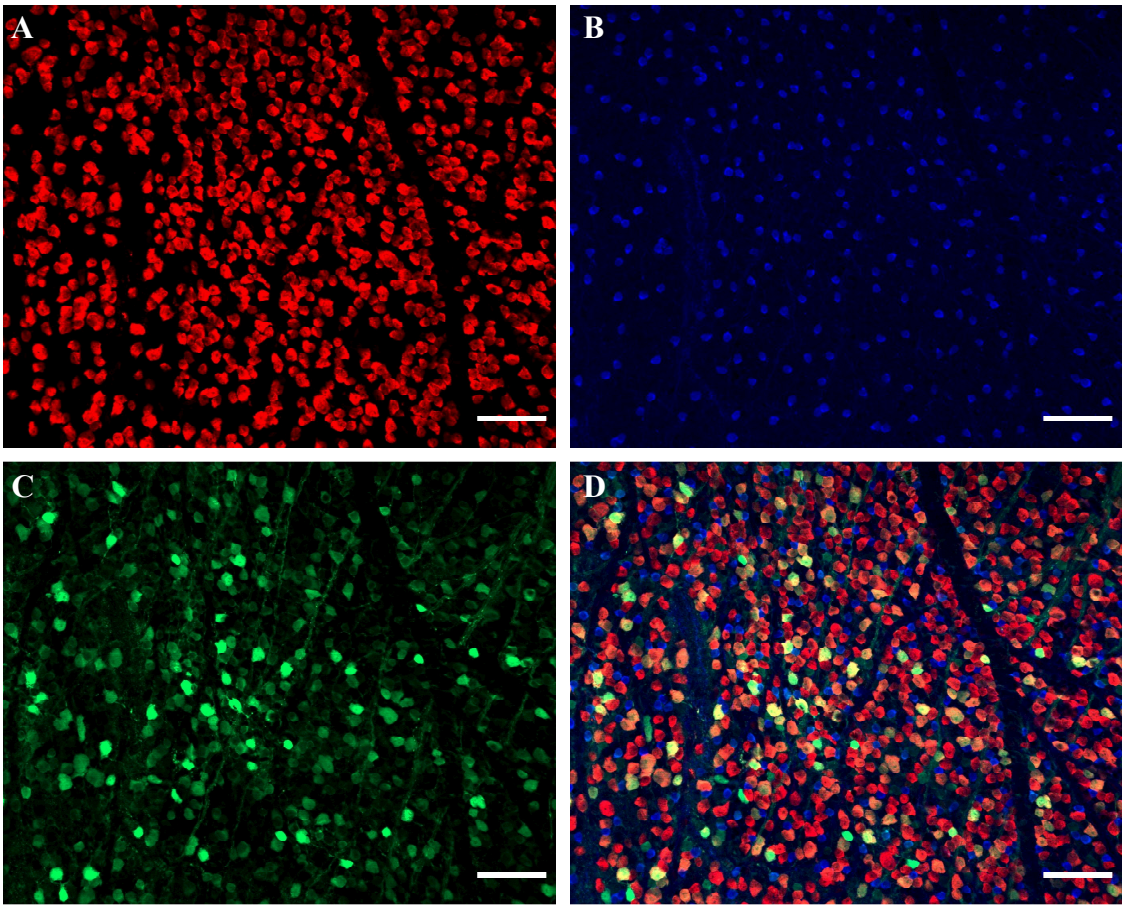

Figure 3.8. Immunohistochemistry of the GCL from a mouse injected with AAV2-CAG-GCaMP3. A) Labelling of RGCs with RNA-binding-protein-multiple-splicing (RBPMS). B) Labelling of amacrine cells with choline acetyltransferase (ChAT). C) Labelling of the virally transduced GCaMP amplified with GFP. D) Merged image with all 3 channels. Scale bars= 50 µm.

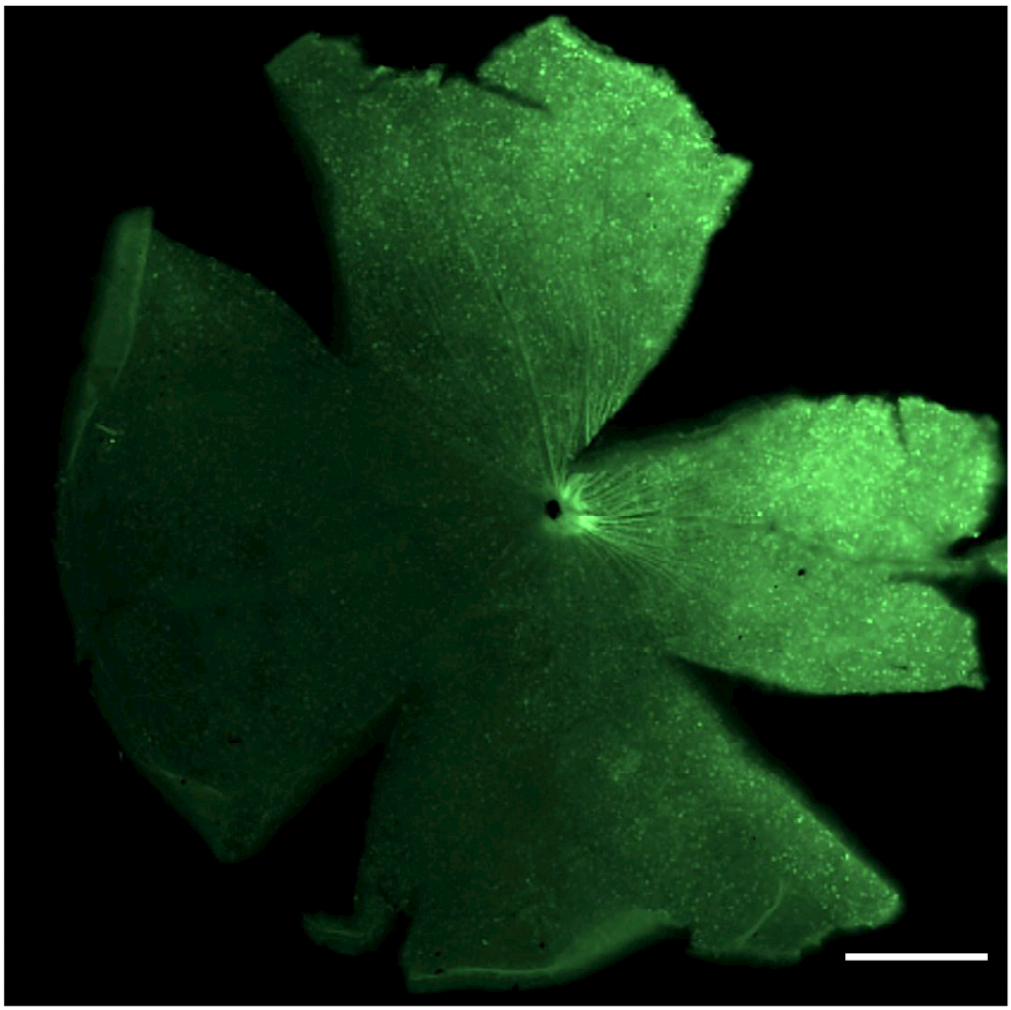

Figure 3.9. GCaMP3 labelling and fluorescence in the superior-temporal retinal region in a mouse injected with AAV2-CAG-GCaMP3. IHC staining for GFP to amplify the GCaMP signal confirmed an injection streak or hot spot of brighter GFP-positive cells closer to the injection site. Scale bar = 1mm.

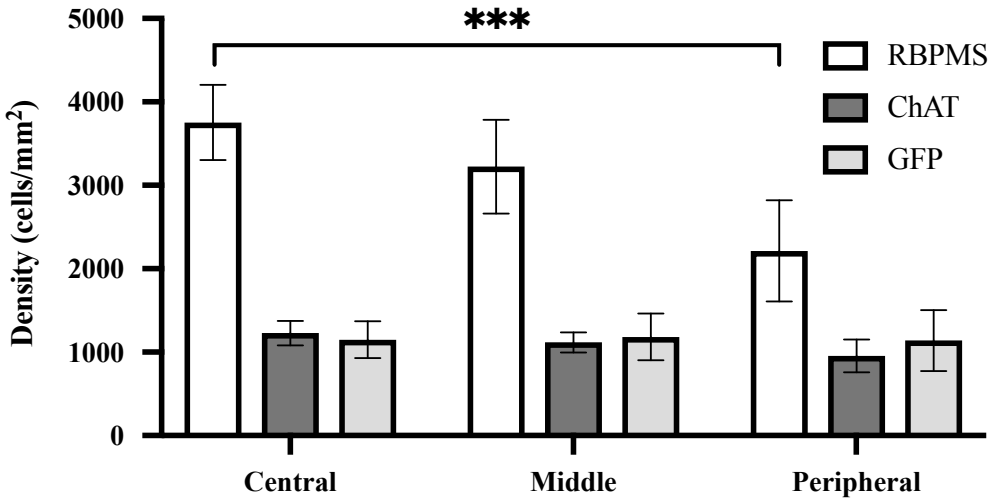

Figure 3.10. Distribution of RBPMS-, ChAT-, and GFP- positive cells with increasing distance from the optic nerve head. Densities of GFP-positive and ChAT-positive cells were evenly distributed in central, middle and peripheral retina. The density of RBPMS-positive cells decreased with increasing distance from the nerve head; $p < 0.005$.

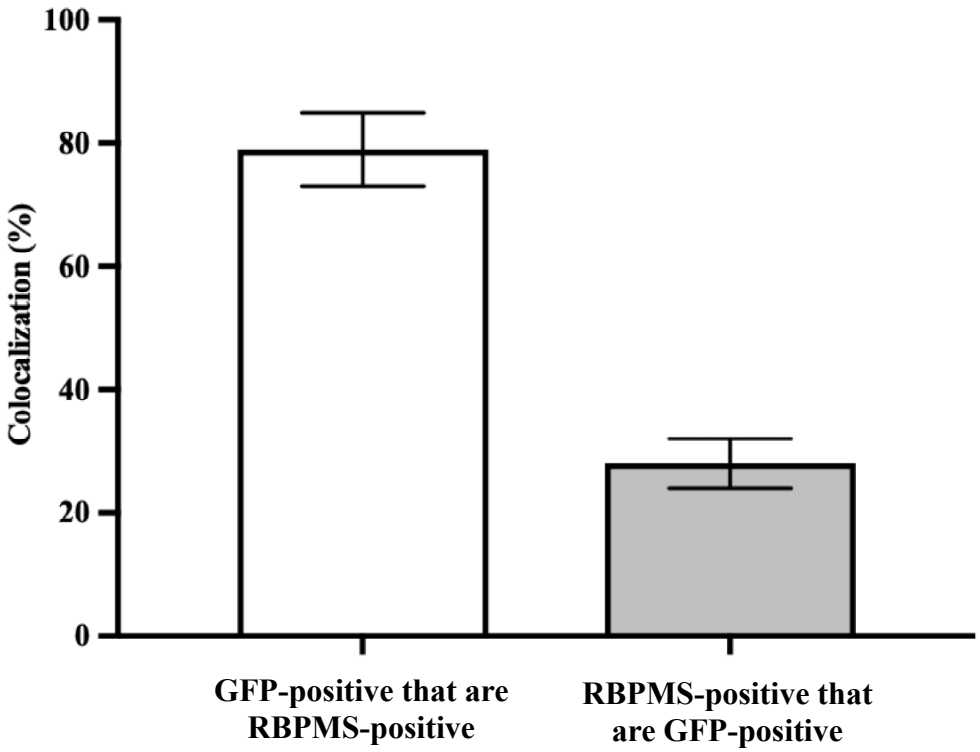

Figure 3.11. Quantification of GCaMP3 colocalization in RBPMS-positive cells in a mouse injected with AAV2-CAG-GCaMP3. Colocalization of GFP-positive and RBPMS-positive cells in the GCL. GFP-positive cells that are RBPMS-positive indicates the specificity of the viral vector to RGCs. RBPMS-positive cells that are GFP-positive indicates the proportion of RGCs that are labelled by the viral vector.

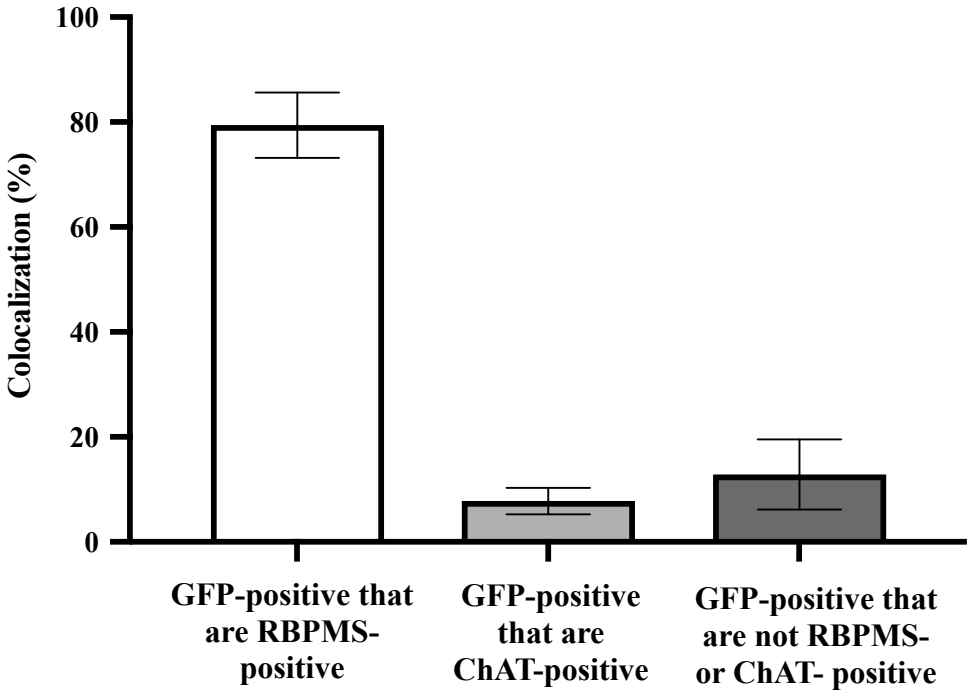

Figure 3.12. Quantification of the GCaMP3 colocalization with retinal cells in a mouse injected with AAV2-CAG-GCaMP3. GFP-positive cells which colocalized with both RBPMS- positive and ChAT-positive cells. A number of GFP-positive cells did not co-localize with either RBPMS or ChAT. Mean (SD) are reported.

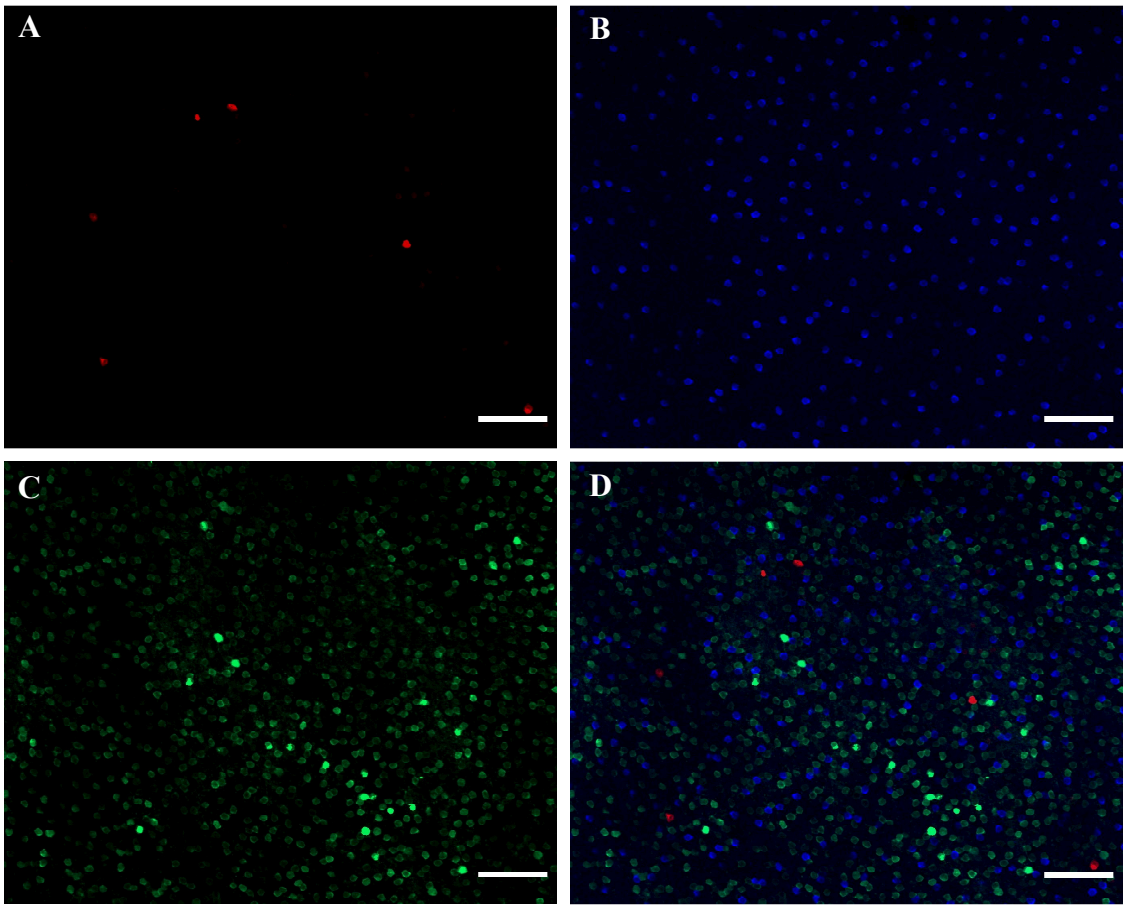

Figure 3.13. Immunohistochemistry of the INL from a mouse injected with AAV2-CAG-GCaMP3. A) Labelling of displaced RGCs with RNA-binding-protein-multiple-splicing (RBPMS). B) Labelling of amacrine cells with choline acetyltransferase (ChAT). C) Labelling of the virally transduced GCaMP amplified with GFP. D) Merged image with all three channels. Scale bars= 50 µm.

CHAPTER 4. Discussion

4.1. Summary of Key Findings

The results of the research presented in this thesis describe the delivery of an exogenous functional fluorescent marker, GCaMP3, to RGCs using a minimally invasive technique. Intravitreal injection of agents, including functional fluorescent markers, is becoming a frequently used technique in eye research as it has relevance to clinical translation for diagnostics and therapeutics. The ability to visualize and quantify RGC function and dysfunction longitudinally is an invaluable tool that will allow greater understanding of the pathophysiology of blinding eye diseases.

The first objective of this thesis characterized the transduction of AAV2-CAG-GCaMP3 into retinal cells using longitudinal *in vivo* imaging. Results showed a significant progressive increase in the number of cells transduced in the GCL across each of the five weeks the mice were imaged following injection. Five weeks was selected for the time-course for monitoring the transduction of the virus from previously published work. Smith and Chauhan injected AAV2-GFP into mice and demonstrated that five weeks of transduction was sufficient to reach a peak in cellular labelling when using the CAG promoter (Smith and Chauhan, 2018). Additional publications have suggested that optimal transduction time can be between two- and eight-weeks post-injection when performing both *ex vivo* and *in vivo* experiments, although the rate of transduction of the virus was not quantified over time in these studies (Borghuis et al., 2011; Weitz et al., 2013; Bar-Noam et al., 2016; Cheong et al., 2018b).

Smith and Chauhan found significant increases in the number of virally transduced cells with AAV2-CAG-GFP until four-weeks post-injection, at which point

the number of labelled cells began to plateau. In contrast to their findings, the number of cells transduced by the AAV2-CAG-GCaMP3 virus in this study increased significantly every week over five weeks following intravitreal injection and no plateau was observed. The mean *in vivo* cell density in their study at four weeks post-injection when the plateau began, was reported as 534 (201) cells/mm^2. In this study, the cellular density of labelled cells at the last timepoint of five weeks following injection was 586 (67) cells/mm^2, therefore, it is possible that if imaged an additional week the mice would have showed a plateau in the number and density of cells transduced.

We observed that GCaMP labelling persisted beyond six months, a finding that to the best of our knowledge, has not been previously reported. This is a significant finding that has an important bearing for longitudinal studies in which long-term behaviour of RGCs is an objective. It is also significant for potential clinical translation in which a method that permits long-term expression of a fluorescent marker that reduces the risk associated with frequent intravitreal injections is desired.

The second objective demonstrated that the GCaMP3 transduced into retinal cells was functional and moreover, demonstrated similar functional properties compared to the Thy1-GCaMP3 transgenic mouse strain previously characterized (Blandford et al., 2019). Although results demonstrated that the KA-induced Ca^{2+} transients in the virus injected group were not significantly different from those in the Thy1-GCaMP3 transgenic mouse group, the transients recorded from the virus injected group had a much greater degree of variability. The most likely reason for this variability is the difference in the quantity of GCaMP transduced and produced within the individual cells. A larger amount of GCaMP could lead to increased baseline fluorescence. In addition, excess GCaMP could act like a Ca^{2+} buffer. As Ca^{2+} is already bound to GCaMP in the cytosol, upon stimulation with

KA there would be less available GCaMP for Ca^{2+} to bind to, thereby potentially leading to a blunted transient response.

Previous work by Borghuis and colleagues found that virally transduced GCaMP3 was able to reliably report consistent Ca^{2+} transients when stimulated optically in an *ex vivo* preparation. They found that although the transduced GCaMP3 had similar kinetic properties when compared to electroporated traditional chemical Ca^{2+} indicators such as Oregon Green BAPTA (OGB), the virally transduced GCaMP3 provided better cellular resolution and specificity to RGCs (Borghuis et al., 2011). Our results demonstrated similar quality cellular resolution and the transduced GCaMP reported consistent transients with chemical stimulation. To our knowledge, it is the first time chemically evoked Ca^{2+} transients are being reported in cells transduced with GCaMP exogenously.

The final objective determined the specificity of the virus to RGCs in the GCL. While labelling was primarily within RGCs, the virus also labelled both cholinergic amacrine cells and another subset of cells that were not RBPMS-positive or ChAT-positive. Labelling of these GFP-positive cells that are not RBPMS- or ChAT-positive in the GCL could be indicative of other subtypes of amacrine cells, such as GABA-ergic amacrine cells (Atan, 2018). The fact that cells, besides RBPMS-positive cells, were labelled was expected because a ubiquitous CAG promotor was used. Although non-specific for RGCs, ubiquitous promotors allow high levels of expression and transduction into retinal cells and are small in size (Dong et al., 1996; Grieger and Samulski, 2005; Hanlon et al., 2017), compared to the cell specific promotors that tend to be larger in size. For example, Thy1 is a promotor specific to RGCs, and is too large in size to be used in AAV vectors due to the packaging capacity of the virial vector (Hanlon et al., 2017). Human-synpasin-1 (hSYN) reportedly has significantly more preferential RGC labelling

compared to other cells in the GCL in rodents, however this finding has not been replicated in non-human primates (NHPs; Borghuis et al., 2011; Yin et al., 2011; Gaub et al., 2014).

Small gene promotors from human DNA, termed “MiniPromotors”, such as DCX, have been developed with the goal of driving more specific expression in inner retinal cells as there is evidence that DCX is expressed in RGCs, as well as in amacrine and bipolar cells (Sànchez-Farìas and Candal, 2015). When DCX was used as the promotor in AAV2 vectors to deliver GFP, it showed more cell specific GFP labelling to RGCs in comparison to other ubiquitous promotors such as CAG (de Leeuw et al., 2014; Smith and Chauhan, 2018). NEFL is another MiniPromotor that when delivered in an AAV vector caused robust labelling in RGCs in NHP retina; primarily in the foveal region as well as portions of the peripheral retina (Hanlon et al., 2017; Simpson et al., 2019).

Lentiviral (LV) vectors are also being developed in attempts to resolve the packaging capacity limitation of transducing larger genes to the retina. LV vectors have an insert capacity of approximately 8 kb in comparison to AAV vectors which are typically limited to less than 4kb (Lundstrom, 2018), making them a potentially more suitable choice depending on the size of the gene being delivered. LV vectors successfully label photoreceptors with intravitreal or subretinal injection (Miyoshi et al., 1997; Takahashi et al., 1999; Kostic et al., 2003), however, their integration into the genome is unstable and inconsistent leading to transient, low and patchy expression in mouse photoreceptors (Kostic et al., 2003). Additionally, labelling is typically only visible close to the injection site (Miyoshi et al., 1997; Greenberg et al., 2006). There are safety concerns surrounding the use of LV vectors as they are based on HIV-1, replicating in both dividing and non-dividing cells. For these reasons, and because the efficacy of

transduction in both photoreceptors and RGCs is better with AAV, AAV still remains the primary choice for gene delivery in the eye and retina (Greenberg et al., 2006).

4.2. Clinical Translation and AAV safety

4.2.1. Gene Therapy in the Retina

The use of AAV as a therapeutic tool in retinal diseases is receiving much recent attention and traction. Currently, there are clinical trials being performed for inherited retinal disorders such as Leber's Congenital Amarurosis (Bainbridge et al., 2008; Bainbridge et al., 2015) and X-Linked Retinoschisis (Cukras et al., 2018).

Leber's Congenital Amaurosis is a hereditary disease resulting in retinal degeneration and subsequent loss of vision. The most common cause of Leber's Congenital Amaurosis occurs from transformations or mutations in the RPE65 gene, which plays a crucial role in the regeneration of visual pigment and the production of 11-cis-retinal (Moiseyev et al., 2005). Without 11-cis-retinal, the photoreceptors cannot respond to light and initiate visual signal transduction through the retina. Bainbridge and colleagues were one of the first research groups to investigate the impact of RPE65 gene therapy in patients with Leber's Congenital Amarurosis. They used an AAV2 vector to deliver the coding sequence of RPE65 to the retina via subretinal injection and patients who received treatment began showing some visual improvement after a few weeks to months following injection (Bainbridge et al., 2008; Bennett et al., 2012; Bainbridge et al., 2015; Pierce and Bennett, 2015; Bennett et al., 2016).

In X-linked Retinoschisis, there are mutations in the RS1 gene, which leads to abnormal splitting between retinal layers (schisis), most frequently in the macula, and abnormalities in the b-wave amplitude in electroretinograms (ERG; b-wave amplitude is

indicative of bipolar cell function; Pepperberg et al., 1978; Cukras et al., 2018). Research has proposed that the abnormal b-wave response is due to loss of signalling function from the photoreceptors to bipolar cells (Ou et al., 2015) because RS1 is important in the maintenance of structural connections of postsynaptic elements between the photoreceptors and bipolar cells (Reid et al., 1999; Molday et al., 2001; Takada et al., 2008; Ou et al., 2015). Preliminary work in RS1-knockout mice has shown that delivery of RS1 with an AAV vector via intravitreal injection can lead to closure of macular schisis and an improvement in the synaptic connections between photoreceptors and bipolar cells, leading to improved signalling (Bush et al., 2016). In preclinical trials, an intravitreal injection of AAV8-RS1 led to visual improvements in RS1 knock-out mice for at least nine months following injection (Bush et al., 2016). In phase I/II clinical trials, schisis closure was reported, demonstrating that this approach could be a future avenue for treating inherited retinal disorders (Cukras et al., 2018).

4.2.2. Current Challenges Facing Clinical Translation

As the intravitreal injection technique continues to be developed as a delivery method for not only gene therapies but also for delivering fluorescent structural and functional markers, there are a number of hurdles that need to be addressed such as neutralizing antibodies to AAV serotypes, the inner limiting membrane thickness in humans, and an increased number of safety studies. Although intravitreal injections are being used clinically to deliver treatments for mutated genes in blind human patients, further research still needs to be performed before exogenous fluorescent proteins can be delivered in humans.

Translation to humans is made difficult by host barriers such as neutralizing antibodies found in the patient population to certain AAV serotypes. For example, over 50% of the population has pre-existing neutralizing antibodies (NAbs) to AAV2, in comparison to other serotypes such as AAV1, -5, -6, -7, and -8 that have a lower prevalence of NAbs (Li et al., 2012; Hemphill et al., 2014). Moreover, different serotypes often have a high degree of similar capsid proteins, leading to NAbs for one serotype cross-reacting with other serotypes (Guo et al., 2018). The fact that NAbs against AAV vectors can block and greatly impair transduction efficacy is a large limitation and as a result, efforts are being made in capsid design, such as using and developing polymers to cover the AAV capsid, thereby blocking NAb recognition and increasing transduction (Carlisle et al., 2008).

Another host barrier is the inner limiting membrane (ILM), which is significantly thicker in humans and NHPs in comparison to rodents (Dalkara et al., 2009). As such, it is hypothesized that if injected intravitreally into humans, the virus would not be able to, or at best only partially be able to, penetrate the ILM and be transduced into retinal cells. In NHPs, intravitreal injections of fluorescent markers such as GFP resulted in labelling that was visibly patchy and typically restricted to the central macula (Yin et al., 2011; Yin et al. 2014). The ILM and RNFL are thinnest in the central fovea and it is possible that this allows the virus to successfully penetrate these physical barriers to permit transduction in RGCs in this region.

There are surgical interventions that could remove the ILM to improve penetrance of the virus into the retina, however, they typically pose a large risk to the integrity of the inner retina as they are quite invasive and damaging. Some of these techniques include peeling of the ILM from the RNFL, and enzymatic degradation of the ILM (Dalkara et

al., 2009; Cehajic-Kapetanovic et al., 2011; Takahashi et al., 2018). Because these methods are quite invasive, other methods that will allow the viral vectors to pass the ILM more efficiently have to be engineered for there to be a higher degree of successful cellular labelling of the inner retinal cells in both NHPs and eventually humans.

4.2.3. Safety of AAV Gene Therapy

Safety studies and characterization of immune responses in the eye are crucial for clinical translation. The eye is immune privileged; however, it is highly immune competent. Immune privilege in the eye refers to the fact that antigens can be introduced in the eye without eliciting as significant an immune response as would be seen following systemic presentation. However, the eye is also immune competent, meaning that it can and is capable of eliciting and producing an immune response upon exposure to a foreign antigen.

The concept of immune privilege was first described following an experiment where a researcher placed a foreign tissue graft in the anterior chamber of the eye and noticed that it was not rejected (Medawar, 1948; Zhou and Caspi, 2010). It is thought that the immune privilege of the eye is due to physical barriers and the ocular microenvironment. The physical barriers include the blood-retina barrier and the lack of lymphatic flow in the eye, acting to prevent larger cells and molecules in and out of the eye. For example, the eye has evolved to not allow for complement-fixing antibodies, neutrophils and macrophages that are relatively large in size to be excluded from the eye to prevent lesions and opacities from forming (Willett and Bennett, 2013). The microenvironment of the eye has also been studied, and researchers Kaplan and Steilein were able to demonstrate that if a foreign antigen was placed into the anterior chamber,

there is activation of suppressor immunity (suppression of T cells) that occurs from the microenvironment containing both cell bound and soluble immunosuppressive factors such as TGF- β, VIP, and α-MSH (Kaplan and Streilein, 1977; Taylor, 2009; Zhao and Caspi, 2010).

Although the eye is regarded as immune privileged it still has an active immune regulatory network that when activated in response to intravitreal injections can pose problems. Problems can include potential damage to ocular structures from the influx of immune cells, and the potential inactivation of the viral vector leading to lower levels of transduction into retinal cells. Following the introduction of a foreign antigen into the eye, there is an immediate response from T helper and T regulatory cells which secrete various cytokines such as Interferon γ (IFNγ), IL-4, IL-10, and IL-13 (Willett and Bennett, 2013). The extent of immune response and immune activation varies according to the antigen presented and its quantity.

Research from pre-clinical and phase I/II clinical trials, report varying ocular immune responses observed in participants following intravitreal or subretinal injections of AAV vectors. In clinical trials for Leber's Congenital Amaurosis, patients were treated with a systemic immunosuppressant and varying quantities of the viral vector. In some patients who received lower doses of the vector, there was no clinically significant immune response detected, while five of eight patients who received higher doses had detectable levels of intraocular inflammation and inflammatory responses (Bainbridge et al., 2015). Although there were no clinically significant responses in the patients who received the lower dose, there was still circulating IFNγ in the peripheral blood (Bainbridge et al., 2008; Bainbridge et al., 2015). These trials concluded that the

increased dose yielded the best results in visual improvement, however, at the cost of higher levels of inflammation that had to be treated over a number of weeks or months.

In clinical trials for X-Linked Retinoschisis, immune responses were detectable as early as two weeks following injection, with the majority of patients experiencing varying levels of ocular inflammation and vitritis by four weeks following injection (Cukras et al., 2018). The inflammation had to be treated with oral and ocular tropical corticosteroids to help resolve the inflammation, which presented as vitreous haze and in severe cases retinal venous leakage and vitreal detachment. The immune responses and T cell activation resolved over approximately two months, with no significant detriments to visual acuity as a result of the inflammation (Cukras et al., 2018). Cukras and colleagues also tested for T cell cytokine production and found that in one patient (one of nine participants), who had the highest level of vitritis also had the highest level of IFNγ when immune assays were performed with peripheral blood testing.

There have also been animal studies in both rodents and NHPs demonstrating the immune response following intravitreal injection of structural markers such as AAV-GFP. Following intravitreal injection of AAV2-CBA-GFP, NAbs to AAV were detected in the blood. A second injection in the same eye or even an injection in the contralateral eye which had not previously experienced an AAV injection, prevented the transduction into retinal cells due to circulating pre-existing NAbs (Li et al., 2008, Kotterman et al., 2015). Furthermore, there appears to be inter-strain differences in mice that exhibit varying immune response severities following AAV injection. Specifically, the C57Bl/6 mouse appears less immunogenic than other strains such as the BALB/c mouse in response to AAV injection (Skelton et al., 2001), which are known to produce robust immune responses (Stripecke et al., 1999; Toguri, 2015). Immune responses following

intravitreal injection of AAV are not only being detected with immune assays, but also by imaging injected mice with OCT and quantifying the amount of inflammation indicated by hyper-reflective or bright spots, in contrast to the dark vitreous background over time (Liu et al., 2020).

The immune response can be decreased if more than one injection at lower doses is performed, however, this can lead to an increase in NAbs, resulting in a lower transduction rate (Li et al., 2008; Kotterman et al., 2015). Currently, the most efficacious method of dampening the immune response is with systemic immunosuppressants prior to the injection, followed by topical immunosuppressants over the first two to four weeks following injection, however, future research in this important area may yield better insight into the safety and potential toxicity of AAVs and provide targeted immunotherapies for these responses.

4.3. Limitations of the Thesis Research

The first limitation of this work was that the viral vector used for this project had a ubiquitous promoter instead of an RGC specific promotor. With IHC, we showed that displaced amacrine cells were labelled, indicating that during *ex vivo* Ca^{2+} imaging experiments, the responses recorded were most likely from both RGCs and displaced amacrine cells. Since we did not perform experiments that blocked responses from amacrine cells, it was not possible for the separation of the responses from these two populations.

Another limitation was that the KA-induced transient amplitudes were more variable in the virus injected group than the transgenic mouse group. Although a possible explanation for the variability was varying levels of GCaMP produced in the cells,

quantification of GCaMP protein levels with Western blot was not performed in either group to demonstrate that the virally injected retinas had higher levels of the protein.

A final limitation relates to potential bias when ROIs were selected for Ca^{2+} imaging experiments in retinas from the virus-injected group. We observed portions of the retina that exhibited very high baseline fluorescence, indicated by the increased amount of red in the pseudocoloured images in comparison to other virally injected retinas imaged. It is likely that these brighter, hyper-responsive regions were in the superior temporal region of the retina, closer to the injection site. These regions of extremely high baseline fluorescence were excluded from the data set and data analysis for two reasons: first, the 50 μM KA treatments commonly caused these very bright cells to become saturated after one or two treatments, and second, when the retinas were treated with KA, the borders of the individual cells overlapped with each other and could no longer be differentiated.

4.4. Future Directions

4.4.1. Ex Vivo Experiments

There are a number of *ex vivo* experiments that could be performed following the findings presented in this thesis. The first could be to determine the other types of retinal cells being labelled by the virus in the GCL and INL by staining for various neurotransmitters that label different families of amacrine cells in the GCL as well as amacrine cells and bipolar cells in the INL. Some examples include GAD65 (glutamic acid decarboxylase 65), GAD67, or GABA that could be used to label GABAergic amacrine cells in the GCL and INL, in addition to GLYT1 (glycine neurotransmitter

transporter) to label glycinergic amacrine cells or TH (tyrosine hydroxylase) to label dopaminergic amacrine cells in the INL (Atan, 2018).

Future work could expand further on amacrine cell function and the response of the displaced amacrine cell population from the GCL in response to KA and attempt to parse out the signal and their transients from that of RGCs during Ca^{2+} imaging. It may be possible to block the responses from amacrine cell populations by treating the retina with 4,9-anhydro-tetrodotoxin (TTX), which is a blocker of voltage gated Na^{+} channels ($Na_v1.6$; Rosker et al., 2007; Smith, 2017). By determining possible substances that could block the responses of displaced amacrine cells, it would allow for primarily RGC transients to be visualized and quantified, however this would need to be analyzed in *in situ* preparations as the effect of 4,9-anhydro-TTX has on both amacrine cells and RGC responses has not been well characterized in the literature.

Finally, Ca^{2+} imaging was only performed on control retinas from mice injected with the viral vector, however, it would be interesting to analyze and characterize the changes in exogenously transduced GCaMP in response to both acute and chronic forms of optic nerve injury such as ONT or optic nerve crush, and elevated intraocular pressure (IOP) models. This characterization would provide foundational data of both the time-frame and degree of cellular dysfunction expected as we move from *ex vivo* to *in vivo* experiments.

4.4.2. Immune Response Characterization following AAV Injection

While performing the longitudinal *in vivo* imaging to characterize the transduction of the virus, OCT images were acquired weekly to ensure that retinal integrity was maintained. During this time, transient turbulence in the vitreous (known clinically as

vitreous haze) was visible in the OCT images, which could be indicative of the occurrence of an immune response. IR and OCT imaging showed clear vitreous, void of any immune response at baseline, however, at one-week post-injection, there was detectable vitreous haze. This haze resolved between three to four-weeks post-injection with no steroidal or immunosuppressant topical drops applied with the exception of the topical antibacterial drops that the mice received immediately following intravitreal injection. Future work to study and characterize this acute inflammatory immune response to AAV2-GCaMP could prove beneficial. To our knowledge there is only published literature on the immune response following AAV2-GFP injection, and none following AAV2-GCaMP injection. It is possible that it would show similar results to what has been published with GFP, however this data is still lacking, and would be valuable safety data for this field.

Following characterization of the immune response with immunoanalysis, treatment options could be explored to prevent this immune response from occurring. This work should be performed in both C57Bl/6 and BALB/c strains to quantify the inter-stain variability that is known to exist (Skelton et al., 2001).

4.4.3. In Vivo 2-Photon Ophthalmoscopy

2P fluorescence imaging is an emerging tool in biological and biomedical research allowing high penetration depth into tissues, while minimizing phototoxicity and photobleaching compared to other imaging techniques such as confocal microscopy (Benninger and Piston, 2014). In single photon excitation, one photon of light is absorbed by a fluorophore, exciting it from its ground state to a higher energy excited state. Shortly after, the fluorophore relaxes back down to its ground state and in the process, emits a

photon of light (Wolf, 2013). In contrast to single photon excitation, 2P excitation uses two photons of light to stimulate fluorescent molecules. These two photons of light act simultaneously, each photon with half the energy, to excite the fluorescent reporter molecule with the same energy as single photon excitation, but twice the wavelength (Denk, 1995; Benninger and Piston, 2014).

Mice have two types of cone photoreceptors, responding to short and medium wavelengths of light; UV and green light, respectively. In contrast, humans have three types of cone photoreceptors, short, medium and long, that respond to blue, green and red light. In single photon imaging, the common excitation wavelengths of fluorescent indicators are within the same excitation wavelengths of the photoreceptors (M cones in mice and M and L cones in humans). 2P excitation ensures that the excitation wavelength of fluorescent indicators such as GCaMP is outside of the spectral excitation wavelengths of the photoreceptors. For example, GCaMP and the photoreceptors are both excited at ~488 nm with single photon excitation, whereas with 2P excitation, the optimal excitation wavelength of GCaMP is increased to approximately 930 nm (Ouzonov et al., 2019).

The spectra for UV cones and S cones, in mice and humans respectively are overlapping, therefore, when imaging with 2P excitation, blue light can be used to excite these cones, initiating the signal transduction through the retina, allowing for an increase the GCaMP signal. Because this imaging modality is being developed with blue light stimulation, it could be adapted in humans to allow for diagnostic imaging of RGC function and dysfunction over time.

Preliminary work in our laboratory with 2P imaging has demonstrated that the GCaMP3 baseline fluorescence is bright and can be visualized using 2P ophthalmoscopy in both Thy1-GCaMP3 transgenic mice (Kamali et al., 2018) as well as AAV2-CAG-

GCaMP3 injected mice. The next goal of this work would be to characterize baseline responses of these virally labelled RGCs to optical stimulation and then attempt to induce injury models such as ONT or elevated IOP models to characterize the loss of function longitudinally.

4.5. Conclusions

Many blinding retinal diseases are caused by death of RGCs, and therefore, there is a need for a unique manner to study and monitor their function over time. There are numerous *ex vivo* structural imaging techniques that can be used to visualize RGCs such as immunohistochemistry, placing exogenous markers to the superior colliculus, and transgenic mice that express markers through RGC specific promoters and genes. Over time, tools to visualize cellular function became widely utilized such as chemical Ca^{2+} indicators, GECIs, and transgenic mice that express GECIs under the control of RGC specific promotors.

As research in transgenic mice is not directly translatable, researchers have turned to exogenous delivery methods such as AAV vectors to deliver GECIs like GCaMP to the inner retina, importantly RGCs. The results of the work presented in this thesis characterized the use of such delivery techniques, demonstrating that AAV can be delivered to the retina, be visualized with *in vivo* imaging and produce functional proteins capable of responding to external stimulation in RGCs. It provides an invaluable tool for studying the underlying pathological mechanisms of blinding ocular diseases *in vivo* and longitudinally in both control states as well as acute and chronic injury models. It paves the way for developing a translational tool for both diagnostic imaging and monitoring the efficacy of future neuroprotective strategies in clinical medicine.

References

1. Amthor FR, Oyster CW, Takahashi ES. Morphology of on-off direction-selective ganglion cells in the rabbit retina. *Brain Res*. 1984;298(1):187-190.

2. Atan D. Immunohistochemical phenotyping of mouse amacrine cell subtypes. *Methods Mol Biol*. 2018;1753:237-248.

3. Augustine GJ, Charlton MP, Smith SJ. Calcium entry and transmitter release at voltage-clamped nerve terminals of squid. *J Physiol*. 1985;367:163-181.

4. Bainbridge JWB, Mehat MS, Sundaram V, et al. Long-term effect of gene therapy on Leber's congenital amaurosis. *N Engl J Med*. 2015;372(20):1887-1897.

5. Bainbridge JWB, Smith AJ, Barker SS, et al. Effect of gene therapy on visual function in Leber's congenital amaurosis. *N Engl J Med*. 2008;358(21):2231-2239.

6. Balakrishnan B, Jayandharan G. Basic Biology of Adeno-Associated Virus (AAV) Vectors Used in Gene Therapy. *Curr Gene Ther*. 2014;14(2):86-100.

7. Bar-Noam AS, Farah N, Shoham S. Correction-free remotely scanned two-photon in vivo mouse retinal imaging. *Light Sci Appl*. 2016;5(e16007)

8. Bennett J, Ashtari M, Wellman J, et al. Gene therapy: AAV2 gene therapy readministration in three adults with congenital blindness. *Sci Transl Med*. 2012;4(120).

9. Bennett J, Wellman J, Marshall KA, et al. Safety and durability of effect of contralateral-eye administration of AAV2 gene therapy in patients with childhood-onset blindness caused by RPE65 mutations: a follow-on phase 1 trial. *Lancet*. 2016;388(10045):661-672.

10. Benninger RK, Piston DW. Two-photon excitation microscopy for the study of living cells and tissues. *Curr Protoc Cell Biol*. 2013;Chapter 4:Unit-4.11.24.

11. Berkelaar M, Clarke DB, Wang YC, Bray GM, Aguayo AJ. Axotomy results in delayed death and apoptosis of retinal ganglion cells in adult rats. *J Neurosci*. 1994;14(7):4368-4374.

12. Berridge MJ. Neuronal Calcium Signaling. *Neuron.* 1998;21:13-26.

13. Bezprozvanny I, Watras J, Ehrlich BE. Bell-shaped calcium-response curves of lns(l,4,5)P3- and calcium-gated channels from endoplasmic reticulum of cerebellum. *Nature*. 1991;351(6329):751-754.

14. Blandford SN, Hooper ML, Yabana T, Chauhan BC, Baldridge WH, Farrell SRM. Retinal characterization of the thy1-GcaMP3 transgenic mouse line after optic nerve transection. *Investig Ophthalmol Vis Sci*. 2019;60(1):183-191.

15. Bloomfield SA, Dowling JE. Roles of aspartate and glutamate in synaptic transmission in rabbit retina. II. Inner plexiform layer. *J Neurophysiol*. 1985;53(3):714-725.

16. Borghuis BG, Tian L, Xu Y, et al. Imaging light responses of targeted neuron populations in the rodent retina. *J Neurosci*. 2011;31(8):2855-2867.

17. Boulton M, Dayhaw-Barker P. The role of the retinal pigment epithelium: Topographical variation and ageing changes. *Eye*. 2001;15(3):384-389.

18. Brini M, Calì T, Ottolini D, Carafoli E. Neuronal calcium signaling: Function and dysfunction. *Cell Mol Life Sci*. 2014;71(15):2787-2814.

19. Brini M, Carafoli E. Calcium pumps in health and disease. *Physiol Rev*. 2009;89(4):1341-1378.

20. Broussard GJ, Liang R, Tian L. Monitoring activity in neural circuits with genetically encoded indicators. *Front Mol Neurosci*. 2014;7

21. Bush RA, Zeng Y, Colosi P, et al. Preclinical dose-escalation study of intravitreal AAV-RS1 gene therapy in a mouse model of X-linked retinoschisis: Dose-dependent expression and improved retinal structure and function. *Hum Gene Ther*. 2016;27(5):376-389.

22. Carlisle RC, Benjamin R, Briggs SS, et al. Coating of adeno-associated virus with reactive polymers can ablate virus tropism, enable retargeting and provide resistance to neutralising antisera. *J Gene Med*. 2008;10(4):400-411.

23. Catterall WA. Voltage-gated calcium channels. *Cold Spring Harb Perspect Biol*. 2011;3(8):1-23.

24. Cehajic-Kapetanovic J, le Goff MM, Allen A, Lucas RJ, Bishop PN. Glycosidic enzymes enhance retinal transduction following intravitreal delivery of AAV2. *Mol Vis*. 2011;17:1771-1783.

25. Chapot CA, Euler T, Schubert T. How do horizontal cells 'talk' to cone photoreceptors? Different levels of complexity at the cone–horizontal cell synapse. *J Physiol*. 2017;595(16):5495-5506.

26. Chauhan BC, Stevens KT, Levesque JM, et al. Longitudinal in vivo imaging of retinal ganglion cells and retinal thickness changes following optic nerve injury in mice. *PLoS One*. 2012;7(6).

27. Chen Q, Cichon J, Wang W, et al. Imaging Neural Activity Using Thy1-GCaMP Transgenic Mice. *Neuron*. 2012;76(2):297-308.

28. Chen Y, Naito J. A quantitative analysis of cells in the ganglion cell layer of the chick retina. *Brain Behav Evol*. 1999;53(2):75-86.

29. Chen TW, Wardill TJ, Sun Y, et al. Ultrasensitive fluorescent proteins for imaging neuronal activity. *Nature*. 2013;499(7458):295-300.

30. Cheong SK, Xiong W, Strazzeri JM, Cepko CL, Williams DR, Merigan WH. In vivo functional imaging of retinal neurons using red and green fluorescent calcium indicators. *Adv Exp Med Biol*. 2018b;1074:135-144

31. Cheong SK, Strazzeri JM, Williams DR, Merigan WH. All-optical recording and stimulation of retinal neurons in vivo in retinal degeneration mice. *PLoS One*. 2018a;13(3):1-20.

32. Colella P, Ronzitti G, Mingozzi F. Emerging Issues in AAV-Mediated In Vivo Gene Therapy. *Mol Ther - Methods Clin Dev*. 2018;8:87-104.

33. Cukras C, Wiley HE, Jeffrey BG, et al. Retinal AAV8-RS1 Gene Therapy for X-Linked Retinoschisis: Initial Findings from a Phase I/IIa Trial by Intravitreal Delivery. *Mol Ther*. 2018;26(9):2282-2294.

34. Curcio CA, Allen KA. Topography of ganglion cells in human retina. *J Comp Neurol*. 1990;300(1):5-25.

35. Dalkara D, Kolstad KD, Caporale N, et al. Inner limiting membrane barriers to aav-mediated retinal transduction from the vitreous. *Mol Ther*. 2009;17(12):2096-2102.

36. de Leeuw CN, Dyka FM, Boye SL, et al. Targeted CNS delivery using human MiniPromoters and demonstrated compatibility with adeno-associated viral vectors. *Mol Ther - Methods Clin Dev*. 2014;1:5.

37. Denk W, Piston DW, Webb WW. Two-Photon Molecular Excitation in Laser-Scanning Microscopy. *Handb Biol Confocal Microsc*. 1995:445-458.

38. Dingledine R, Borges K, Bowie D, Traynelis SF. The glutamate receptor ion channels. *PharmacolRev*. 1999;51(1):7-62.

39. Dong JY, Fan PD, Frizzell RA. Quantitative analysis of the packaging capacity of recombinant adeno-associated virus. *Hum Gene Ther*. 1996;7(17):2101-2112.

40. Ehinger B, Ottersen OP, Storm-Mathisen J, Dowling JE. Bipolar cells in the turtle retina are strongly immunoreactive for glutamate. *Proc Natl Acad Sci U S A*. 1988;85(21):8321-8325.

41. Gao G-P, Alvira MR, Wang L, Calcedo R, Johnston J, Wilson JM. Novel adeno-associated viruses from rhesus monkeys. *Proc Natl Acad SCi*. 2002;99(18):11854-11859.

42. Gaub BM, Berry MH, Holt AE, et al. Restoration of visual function by expression of a light-gated mammalian ion channel in retinal ganglion cells or ON-bipolar cells. *Proc Natl Acad Sci U S A*. 2014;111(51):E5574-E5583.

43. Gee KR, Brown KA, Chen WNU, Bishop-Stewart J, Gray D, Johnson I. Chemical and physiological characterization of fluo-4 Ca^{2+}-indicator dyes. *Cell Calcium*. 2000;27(2):97-106.

44. Greenberg KP, Lee ES, Schaffer D V., Flannery JG. Gene delivery to the retina using lentiviral vectors. *Adv Exp Med Biol*. 2005;572:255-266.

45. Grieger JC, Samulski RJ. Packaging Capacity of Adeno-Associated Virus Serotypes: Impact of Larger Genomes on Infectivity and Postentry Steps. *J Virol*. 2005;79(15):9933-9944.

46. Grienberger C, Konnerth A. Imaging Calcium in Neurons. *Neuron*. 2012;73:862-885.

47. Grynkiewicz G, Poenie M, Tsien RY. A new generation of Ca^{2+} indicators with greatly improved fluorescence properties. *J Biol Chem*. 1985;260(6):3440-3450.

48. Guo P, Zhang J, Chrzanowski M, et al. Rapid AAV-Neutralizing Antibody Determination with a Cell-Binding Assay. *Mol Ther - Methods Clin Dev*. 2019;13:40-46.

49. Ham WT, Mueller HA, Sliney DH. Retinal sensitivity to damage from short wavelength light. *Nature*. 1976;260(5547):153-155.

50. Hanlon KS, Chadderton N, Palfi A, et al. A novel retinal ganglion cell promoter for utility in AAV vectors. *Front Neurosci*. 2017;11.

51. Hauswirth WW. Retinal gene therapy using adeno-associated viral vectors: Multiple applications for a small virus. *Hum Gene Ther*. 2014;25(8):671-678.

52. Hemphill DD, McIlwraith CW, Samulski RJ, Goodrich LR. Adeno-associated viral vectors show serotype specific transduction of equine joint tissue explants and cultured monolayers. *Sci Rep*. 2014;4.

53. Henzi V, MacDermott AB. Characteristics and function of Ca^{2+} - and inositol 1,4,5-trisphosphate-releasable stores of Ca^{2+} in neurons. *Neuroscience*. 1992;46(2):251-273.

54. Ivanova E, Hwang GS, Pan ZH, Troilo D. Evaluation of AAV-mediated expression of chop2-GFP in the marmoset retina. *Investig Ophthalmol Vis Sci*. 2010;51(10):5288-5296.

55. Jares-Erijman EA, Jovin TM. FRET imaging. *Nat Biotechnol*. 2003;21(11):1387-1395.

56. Jeon CJ, Strettoi E, Masland RH. The major cell populations of the mouse retina. *J Neurosci*. 1998;18(21):8936-8946.

57. Kamali T, Fischer J, Farrell S, Baldridge WH, Zinser G, Chauhan BC. Simultaneous in vivo confocal reflectance and two-photon retinal ganglion cell imaging based on a hollow core fiber platform. *J Biomed Opt*. 2018;23(09):1.

58. Kaplan HJ, Streilein JW. Immune response to immunization via the anterior chamber of the eye. I. F. lymphocyte-induced immune deviation. *J Immunol*. 1977;118(3):809-814.

59. Katz B, Miledi R. Ionic requirements of synaptic transmitter release. *Nature*. 1967;215(5101):651.

60. Kolb H. Simple Anatomy of the Retina by Helga Kolb. Webvision The Organization of the Retina and Visual System website. October 8, 2011. Accessed on May 23, 2020.

61. Kolb H, Nelson R, Ahnelt P, Cuenca N. Cellular organization of the vertebrate retina. *Prog Brain Res*. 2001;131:3-26.

62. Kostic C, Chiodini F, Salmon P, et al. Activity analysis of housekeeping promoters using self-inactivating lentiviral vector delivery into the mouse retina. *Gene Ther*. 2003;10(9):818-821.

63. Kostyuk P, Verkhratsky A. Calcium stores in neurons and glia. *Neuroscience*. 1994;63(2):381-404.

64. Kotterman MA, Yin L, Strazzeri JM, Flannery JG, Merigan WH, Schaffer D V. Antibody neutralization poses a barrier to intravitreal adeno-associated viral vector gene delivery to non-human primates. *Gene Ther*. 2015;22(2):116-126.

65. Lee SH, Yang JY, Madrakhimov S, Park HY, Park K, Park TK. Adeno-Associated Viral Vector 2 and 9 Transduction Is Enhanced in Streptozotocin-Induced Diabetic Mouse Retina. *Mol Ther - Methods Clin Dev*. 2019;13(June):55-66.

66. Lei B, Zhang K, Yue Y, Ghosh A, Duan D. Adeno-associated virus serotype-9 efficiently transduces the retinal outer plexiform layer. *Mol Vis*. 2009;15(July):1374-1382.

67. Li C, Narkbunnam N, Samulski RJ, et al. Neutralizing antibodies against adeno-associated virus examined prospectively in pediatric patients with hemophilia. *Gene Ther*. 2012;19(3):288-294.

68. Li Q, Miller R, Han PY, et al. Intraocular route of AAV2 vector administration defines humoral immune response and therapeutic potential. *Mol Vis*. 2008;14:1760-1769.

69. Liu YF, Huang S, Ng TK, et al. Longitudinal evaluation of immediate inflammatory responses after intravitreal AAV2 injection in rats by optical coherence tomography. *Exp Eye Res*. 2020;193.

70. Lundstrom K. Viral Vectors in Gene Therapy. *Diseases*. 2018;6(2).

71. Lüscher C, Huber KM. Group 1 mGluR-Dependent Synaptic Long-Term Depression: Mechanisms and Implications for Circuitry and Disease. *Neuron*. 2010;65(4):445-459.

72. Lüscher C, Malenka RC. NMDA receptor-dependent long-term potentiation and long-term depression (LTP/LTD). *Cold Spring Harb Perspect Biol*. 2012;4(6):a005710.

73. Lyons MR, West AE. Mechanisms of specificity in neuronal activity-regulated gene transcription. *Prog Neurobiol*. 2011;94(3):259-295.

74. Marc RE, Liu WLS, Kalloniatis M, Raiguel SF, Van Haesendonck E. Patterns of glutamate immunoreactivity in the goldfish retina. *J Neurosci*. 1990;10(12):4006-4034.

75. Marchi S, Pinton P. The mitochondrial calcium uniporter complex: Molecular components, structure and physiopathological implications. *J Physiol*. 2014;592(5):829-839.

76. Meinrenken CJ, Borst JGG, Sakmann B. Local routes revisited: The space and time dependence of the Ca^{2+} signal for phasic transmitter release at the rat calyx of Held. *J Physiol*. 2003;547(3):665-689.

77. Meissner G. Ryanodine activation and inhibition of the Ca^{2+} release channel of sarcoplasmic reticulum. *J Biol Chem*. 1986;261(14):6300-6306.

78. Miyawaki A, Llopis J, Heim R, et al. Fluorescent indicators for Ca^{2+} based on green fluorescent proteins and calmodulin. *Nature*. 1997;388(6645):882-887.

79. Miyoshi H, Takahashi M, Gage FH, Verma IM. Stable and efficient gene transfer into the retina using an HIV-based lentiviral vector. *Proc Natl Acad Sci U S A*. 1997;94(19):10319-10323.

80. Moiseyev G, Chen Y, Takahashi Y, Wu BX, Ma JX. RPE65 is the isomerohydrolase in the retinoid visual cycle. *Proc Natl Acad Sci U S A*. 2005;102(35):12413-12418.

81. Molday LL, Hicks D, Sauer CG, Weber BHF, Molday RS. Expression of X-linked retinoschisis protein RS1 in photoreceptor and bipolar cells. *Investig Ophthalmol Vis Sci*. 2001;42(3):816-825.

82. Nakai J, Ohkura M, Imoto K. A high signal-to-noise ca^{2+} probe composed of a single green fluorescent protein. *Nat Biotechnol*. 2001;19(2):137-141.

83. Neher E, Sakaba T. Multiple Roles of Calcium Ions in the Regulation of Neurotransmitter Release. *Neuron*. 2008;59(6):861-872.

84. Niswender CM, Conn PJ. Metabotropic Glutamate Receptors: Physiology, Pharmacology, and Disease. *Annu Rev Pharmacol Toxicol*. 2010;50(1):295-322.

85. Ochakovski GA, Ulrich Bartz-Schmidt K, Fischer MD. Retinal gene therapy: Surgical vector delivery in the translation to clinical trials. *Front Neurosci*. 2017;11(APR):1-7.

86. Ou J, Vijayasarathy C, Ziccardi L, et al. Synaptic pathology and therapeutic repair in adult retinoschisis mouse by AAV-RS1 transfer. *J Clin Invest*. 2015;125(7):2891-2903.

87. Ouzounov DG, Wang T, Wu C, Xu C. GCaMP6 ΔF/F dependence on the excitation wavelength in 3-photon and 2-photon microscopy of mouse brain activity. *Biomed Opt Express*. 2019;10(7):3343.

88. Palty R, Silverman WF, Hershfinkel M, et al. NCLX is an essential component of mitochondrial Na^+/Ca^{2+} exchange. *Proc Natl Acad Sci U S A*. 2010;107(1):436-441.

89. Paredes RM, Etzler JC, Watts LT, Lechleiter JD. Chemical Calcium Indicatiors. *Imaging*. 2009;46(3):143-151.

90. Pepperberg DR, Brown PK, Lurie M, Dowling JE. Visual pigment and photoreceptor sensitivity in the isolated skate retina. *J Gen Physiol*. 1978;71(4):369-396.

91. Pérez Koldenkova V, Nagai T. Genetically encoded Ca^{2+} indicators: Properties and evaluation. *Biochim Biophys Acta - Mol Cell Res*. 2013;1833(7):1787-1797.

92. Pierce EA, Bennett J. The status of RPE65 gene therapy trials: Safety and efficacy. *Cold Spring Harb Perspect Med*. 2015;5(9).

93. Porumb T, Yau P, Harvey TS, Ikura M. A calmodulin-target peptide hybrid molecule with unique calcium-binding properties. *Protein Eng Des Sel*. 1994;7(1):109-115.

94. Qin Z, He S, Yang C, et al. Adaptive optics two-photon microscopy enables near-diffraction-limited and functional retinal imaging in vivo. *Light Sci Appl*. 2020;9(1).

95. Quigley HA, Davis EB, Anderson DR. Descending optic nerves degeneration in primates. *Investig Ophthalmol Vis Sci*. 1977;16(9):841-849.

96. Reid SNM, Akhmedov NB, Piriev NI, Kozak CA, Danciger M, Farber DB. The mouse X-linked juvenile retinoschisis cDNA: Expression in photoreceptors. *Gene*. 1999;227(2):257-266.

97. Roderick HL, Berridge MJ, Bootman MD. Calcium-induced calcium release. *Curr Biol*. 2003;13(11).

98. Rosker C, Lohberger B, Hofer D, Steinecker B, Quasthoff S, Schreibmayer W. The TTX metabolite 4,9-anhydro-TTX is a highly specific blocker of the Nav1.6 voltage-dependent sodium channel. *Am J Physiol - Cell Physiol*. 2007;293(2).

99. Sabatini BL, Regehr WG. Timing of neurotransmission at fast synapses in the mammalian brain. *Nature*. 1996;384(6605):170-172.

100. Sánchez-Farías N, Candal E. Doublecortin is widely expressed in the developing and adult retina of sharks. *Exp Eye Res*. 2015;134:90-100.

101. Sanes JR, Zipursky SL. Design Principles of Insect and Vertebrate Visual Systems. *Neuron*. 2010;66(1):15-36.

102. Schwaller B. Cytosolic Ca^{2+} buffers. *Cold Spring Harb Perspect Biol*. 2010;2(11).

103. Sekar RB, Periasamy A. Fluorescence resonance energy transfer (FRET) microscopy imaging of live cell protein localizations. *J Cell Biol*. 2003;160(5):629-633.

104. Sharma R, Yin L, Geng Y, et al. In vivo two-photon imaging of the mouse retina. *Biomed Opt Express*. 2013;4(8):1285.

105. Simpson EM, Korecki AJ, Fornes O, et al. New MiniPromoter Ple345 (NEFL) drives strong and specific expression in retinal ganglion cells of mouse and primate retina. *Hum Gene Ther*. 2019;30(3):257-272.

106. Simpson PB, John Challiss RA, Nahorski SR. Neuronal Ca^{2+} stores: activation and function. *Trends Neurosci*. 1995;18(7):299-306.

107. Slaughter MM, Miller RF. The role of excitatory amino acid transmitters in the mudpuppy retina: An analysis with kainic acid and N-methyl aspartate. *J Neurosci*. 1983;3(8):1701-1711.

108. Smerdon D. Anatomy of the eye and orbit. *Curr Anaesth Crit Care*. 2000;11(6):286-292.

109. Smith B. Contribution of Na(v) channels to the development and function of the retina [dissertation]. Dalhousie University; 2017.

110. Smith CA, Chauhan BC. In vivo imaging of adeno-associated viral vector labelled retinal ganglion cells. *Sci Rep*. 2018;8(1):1-11.

111. Stripecke R, Del Carmen Villacres M, Skelton DC, Satake N, Halene S, Kohn DB. Immune response to green fluorescent protein: Implications for gene therapy. *Gene Ther*. 1999;6(7):1305-1312.

112. Südhof TC. Calcium control of neurotransmitter release. *Cold Spring Harb Perspect Biol*. 2012;4(1).

113. Takada Y, Vijayasarathy C, Zeng Y, Kjellstrom S, Bush RA, Sieving PA. Synaptic pathology in retinoschisis knockout (Rs1-/y) mouse retina and modification by rAAV-Rs1 gene delivery. *Investig Ophthalmol Vis Sci*. 2008;49(8):3677-3686.

114. Takahashi K, Igarashi T, Miyake K, et al. Improved Intravitreal AAV-Mediated Inner Retinal Gene Transduction after Surgical Internal Limiting Membrane Peeling in Cynomolgus Monkeys. *Mol Ther*. 2017;25(1):296-302.

115. Takahashi M, Miyoshi H, Verma IM, Gage FH. Rescue from Photoreceptor Degeneration in the rd mouse by Human Immunodeficiency Virus Vector-Mediated Gene Transfer. *J Virol*. 1999;73(9):7812-7816.

116. Taylor AW. Ocular immune privilege. *Eye*. 2009;23(10):1885-1889.

117. Tian L, Hires SA, Mao T, et al. Imaging neural activity in worms, flies and mice with improved GCaMP calcium indicators. *Nat Methods*. 2009;6(12):875-881.

118. Toguri JT. Endocannabinoid system modulation of the ocular immune response. 2015

119. Tsien RY. New Calcium Indicators and Buffers with High Selectivity Against Magnesium and Protons: Design, Synthesis, and Properties of Prototype Structures. *Biochemistry*. 1980;19(11):2396-2404.

120. Wässle H. Parallel processing in the mammalian retina. *Nat Rev Neurosci*. 2004;5(10):747-757.

121. Weitz AC, Behrend MR, Lee NS, et al. Imaging the response of the retina to electrical stimulation with genetically encoded calcium indicators. *J Neurophysiol*. 2013;109(7):1979-1988.

122. Werblin FS, Dowling JE. Organization of the retina of the mudpuppy, Necturus maculosus. II. Intracellular recording. *J Neurophysiol*. 1969;32(3):339-355.

123. Whitaker M. Genetically encoded probes for measurement of intracellular calcium. *Methods Cell Biol*. 2010;99(C):153-182.

124. Willett K, Bennett J. Immunology of AAV-mediated gene transfer in the eye. *Front Immunol*. 2013;4.

125. Wolf DE. Fundamentals of fluorescence and fluorescence microscopy. *Methods Cell Biol*. 2013;114:69-97.

126. Ye L, Haroon MA, Salinas A, Paukert M. Comparison of GCaMP3 and GCaMP6f for studying astrocyte Ca^{2+} dynamics in the awake mouse brain. 2017:1-17.

127. Yin L, Geng Y, Osakada F, et al. Imaging light responses of retinal ganglion cells in the living mouse eye. *J Neurophysiol*. 2013;109(9):2415-2421.

128. Yin L, Greenberg K, Hunter JJ, et al. Intravitreal injection of AAV2 transduces macaque inner retina. *Investig Ophthalmol Vis Sci*. 2011;52(5):2775-2783.

129. Yin L, Masella B, Dalkara D, et al. Imaging light responses of foveal ganglion cells in the living macaque eye. *J Neurosci*. 2014;34(19):6596-6605.

130. Zhao Y, Araki S, Wu J, et al. An expanded palette of genetically encoded Ca^{2+} indicators. *Science*. 2011;333(6051):1888-1891.

131. Zhou R, Caspi RR. Ocular immune privilege. *F1000 Biol Rep*. 2010;2(1).

132. Zincarelli C, Soltys S, Rengo G, Rabinowitz JE. Analysis of AAV serotypes 1-9 mediated gene expression and tropism in mice after systemic injection. *Mol Ther*. 2008;16(6):1073-1080.

133. Zucker RS. Calcium- and activity-dependent synaptic plasticity. *Curr Opin Neurobiol*. 1999;9(3):305-313.

Appendix A: Copyright Permissions

INTRODUCTION

Figure 1.1.

ELSEVIER LICENSE
TERMS AND CONDITIONS

Jul 22, 2020

This Agreement between Ms. Delaney Henderson ("You") and Elsevier ("Elsevier") consists of your license details and the terms and conditions provided by Elsevier and Copyright Clearance Center.

License Number	4863080435274
License date	Jul 06, 2020
Licensed Content Publisher	Elsevier
Licensed Content Publication	Current Anaesthesia & Critical Care
Licensed Content Title	Anatomy of the eye and orbit
Licensed Content Author	D. Smerdon
Licensed Content Date	Dec 1, 2000
Licensed Content Volume	11
Licensed Content Issue	6
Licensed Content Pages	7
Start Page	286
End Page	292
Type of Use	reuse in a thesis/dissertation
Portion	figures/tables/illustrations
Number of figures/tables/illustrations	1

Figure 1.2.

SPRINGER NATURE LICENSE
TERMS AND CONDITIONS

Jul 22, 2020

This Agreement between Ms. Delaney Henderson ("You") and Springer Nature ("Springer Nature") consists of your license details and the terms and conditions provided by Springer Nature and Copyright Clearance Center.

License Number	4863100457281
License date	Jul 06, 2020
Licensed Content Publisher	Springer Nature
Licensed Content Publication	Nature Reviews Neuroscience
Licensed Content Title	Understanding the retinal basis of vision across species
Licensed Content Author	Tom Baden et al
Licensed Content Date	Nov 28, 2019
Type of Use	Thesis/Dissertation
Requestor type	non-commercial (non-profit)
Format	print and electronic
Portion	figures/tables/illustrations
Number of figures/tables/illustrations	1
High-res required	no
Will you be translating?	no
Circulation/distribution	1 - 29

Figure 1.3.

ELSEVIER LICENSE
TERMS AND CONDITIONS

Jul 22, 2020

This Agreement between Ms. Delaney Henderson ("You") and Elsevier ("Elsevier") consists of your license details and the terms and conditions provided by Elsevier and Copyright Clearance Center.

License Number	4863080863461
License date	Jul 06, 2020
Licensed Content Publisher	Elsevier
Licensed Content Publication	Neuron
Licensed Content Title	Imaging Calcium in Neurons
Licensed Content Author	Christine Grienberger,Arthur Konnerth
Licensed Content Date	Mar 8, 2012
Licensed Content Volume	73
Licensed Content Issue	5
Licensed Content Pages	24
Start Page	862
End Page	885
Type of Use	reuse in a thesis/dissertation
Portion	figures/tables/illustrations
Number of figures/tables/illustrations	1